Cell Reports

Article

Ubiquitylation of the ER-Shaping Protein Lunapark via the CRL3^{KLHL12} Ubiquitin Ligase Complex

Graphical Abstract

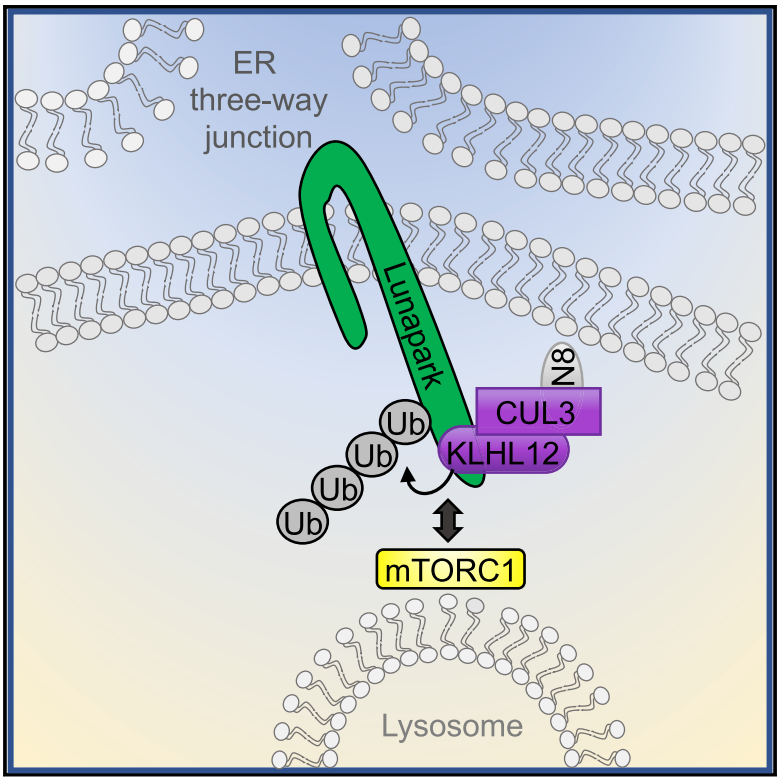

Authors

Laurensia Yuniati, Angela Lauriola, Manouk Gerritsen, ..., Andrea Vettori, Timothy Cardozo, Daniele Guardavaccaro

Correspondence

daniele.guardavaccaro@univr.it

In Brief

Yuniati et al. perform a proteomic screen to identify E3 substrates that are ubiquitylated at cellular membranes and find that the ER-shaping protein Lunapark is ubiquitylated by the CRL3^{KLHL12} ubiquitin ligase. They show that Lunapark binds mTORC1 and affects its activity, and defects in Lunapark ubiquitylation lead to neurodevelopmental defects.

Highlights

- A proteomic approach to identify CRL substrates ubiquitylated at cellular membranes
- The ER shaping protein Lunapark is ubiquitylated by the CRL3^{KLHL12} ubiquitin ligase
- Lunapark binds mTOR and its ubiquitylation affects lysosomal recruitment of mTORC1
- Inhibition of Lunapark ubiquitylation leads to neurodevelopmental defects

Yuniati et al., 2020, Cell Reports *31*, 107664
May 19, 2020
https://doi.org/10.1016/j.celrep.2020.107664

CellPress

Cell Reports

CellPress
OPEN ACCESS

Article

Ubiquitylation of the ER-Shaping Protein Lunapark via the CRL3^{KLHL12} Ubiquitin Ligase Complex

Laurensia Yuniati,[1,7] Angela Lauriola,[2,7] Manouk Gerritsen,[1] Susana Abreu,[1] Eric Ni,[3] Chiara Tesoriero,[2] Jacob O. Onireti,[2] Teck Yew Low,[4] Albert J.R. Heck,[5,6] Andrea Vettori,[2] Timothy Cardozo,[3] and Daniele Guardavaccaro[1,2,8,*]

[1]Hubrecht Institute-KNAW and University Medical Center Utrecht, 3584 CT Utrecht, the Netherlands
[2]Department of Biotechnology, University of Verona, 37134 Verona, Italy
[3]Department of Biochemistry and Molecular Pharmacology, New York University School of Medicine, NYU Langone Health, New York, NY 10016, USA
[4]UKM Medical Molecular Biology Institute (UMBI), Universiti Kebangsaan Malaysia, 56000 Kuala Lumpur, Malaysia
[5]Biomolecular Mass Spectrometry and Proteomics, Bijvoet Center for Biomolecular Research and Utrecht Institute for Pharmaceutical Sciences, Utrecht University, 3584 CH Utrecht, the Netherlands
[6]The Netherlands Proteomics Center, 3584 CH Utrecht, the Netherlands
[7]These authors contributed equally
[8]Lead Contact
*Correspondence: daniele.guardavaccaro@univr.it
https://doi.org/10.1016/j.celrep.2020.107664

SUMMARY

Cullin-RING ligases (CRLs) control key cellular processes by promoting ubiquitylation of a multitude of soluble cytosolic and nuclear proteins. Subsets of CRL complexes are recruited and activated locally at cellular membranes; however, few CRL functions and substrates at these distinct cellular compartments are known. Here, we use a proteomic screen to identify proteins that are ubiquitylated at cellular membranes and found that Lunapark, an endoplasmic reticulum (ER)-shaping protein localized to ER three-way junctions, is ubiquitylated by the CRL3^{KLHL12} ubiquitin ligase. We demonstrate that Lunapark interacts with mechanistic target of rapamycin complex-1 (mTORC1), a central cellular regulator that coordinates growth and metabolism with environmental conditions. We show that mTORC1 binds Lunapark specifically at three-way junctions, and lysosomes, where mTORC1 is activated, make contact with three-way junctions where Lunapark resides. Inhibition of Lunapark ubiquitylation results in neurodevelopmental defects indicating that KLHL12-dependent ubiquitylation of Lunapark is required for normal growth and development.

INTRODUCTION

Cullin-RING ligases (CRLs), the largest class of modular E3 ubiquitin ligases, control essential cellular processes by targeting protein substrates for ubiquitylation (Petroski and Deshaies, 2005). CRLs are composed of a cullin scaffold, a RING-finger protein (RBX1 or RBX2), an adaptor protein, and one of many substrate-receptor subunits. CRL activity is promoted by the reversible conjugation of the ubiquitin-like protein NEDD8 to the cullin subunit (Scott et al., 2014). Like ubiquitylation, neddylation of substrates is achieved by an enzymatic cascade. NEDD8 is first activated by specific E1 and E2 enzymes and then conjugated by E3 enzymes to a lysine residue of the cullin target through an isopeptide bond (Lydeard et al., 2013). A "dual E3" mechanism has been proposed for cullin neddylation, where one E3, RBX1, works as a typical E3 by recruiting both the cullin substrate and the E2-NEDD8 intermediate triggering NEDD8 ligation, and a second E3, termed co-E3, facilitates this process (Lydeard et al., 2013; Scott et al., 2010, 2011). This auxiliary scaffold-like co-E3 function is played by defective in Cul neddylation protein (DCN) in yeast and DCNL1 to DCNL5 in humans (DCN-like proteins). DCN and DCN-like proteins interact with the cullin subunit nearby its neddylation site as well as the acetylated N terminus of the E2 enzyme (UBC12) structurally constraining the RBX1-UBC12-NEDD8 complex to orientations that increase the kinetic efficiency of the NEDD8 conjugation to the right lysine residue (Kurz et al., 2005, 2008; Monda et al., 2013). Notably, one DCNL protein, DCNL3, has been shown to be localized to cellular membranes through an N-terminal lipid-modified motif (Keuss et al., 2016; Meyer-Schaller et al., 2009). Membrane-bound DCNL3 recruits CRLs to membranes where it contributes to their neddylation (Keuss et al., 2016; Meyer-Schaller et al., 2009).

The endoplasmic reticulum (ER), the largest membrane-bound organelle in eukaryotes, is a contiguous structure that extends from the nuclear envelope to the plasma membrane (Chen et al., 2013; Friedman and Voeltz, 2011; Phillips and Voeltz, 2016). The ER is composed of two main structural units, namely flat cisternal sheets and reticulated tubules. Whereas the cisternae are connected to the nuclear envelope and are localized mostly to the perinuclear region, the tubules form a polygonal network that extends throughout the cytoplasm. This polygonal array is highly dynamic as it undergoes rapid and constant reorganizations such as tubule extension and retraction, branching,

sliding, ring closure, and tubule-tubule fusion. Key elements of the ER tubule network are three-way junctions, mobile ER intersections generated by the fusion of one ER tubule tip with the side of another tubule. Lunapark, a recently identified factor implicated in ER morphology, is an evolutionarily conserved transmembrane protein that specifically localizes to ER three-way junctions. Although Lunapark is thought to stabilize these junctions and inhibit ring closure (Chen et al., 2012, 2015; Wang et al., 2016), its function and regulation are still poorly understood.

Mechanistic target of rapamycin complex 1 (mTORC1) is an evolutionarily conserved serine-threonine protein kinase complex that controls metabolic processes underlying the growth of cells, tissues, and organs (Saxton and Sabatini, 2017). In response to favorable internal and external cues, mTORC1 is activated to promote anabolic processes such as protein, lipid, and nucleotide synthesis, and inhibit catabolic processes like autophagy. Two independent conditions have to be achieved to activate mTORC1. First, mTORC1 has to transiently translocate to the lysosomal membrane in response to amino acids, a process promoted by the direct binding of activated Rag GTPases to Raptor, which forms a stoichiometric complex with mTOR and associates with the mTOR substrates eukaryotic initiation factor 4E-binding protein-1 and ribosomal protein S6 kinase (Kim et al., 2008; Manifava et al., 2016; Sancak et al., 2008; Sekiguchi et al., 2001). Second, lysosome-localized mTORC1 has to interact with Ras homolog enriched in brain (Rheb), a small GTPase that is activated in response to growth factors. Thus, the lysosome represents the cellular hub where the amino acid- and growth factor-sensing machineries intersect to activate mTORC1.

In this study, we have carried out a screen aimed at the identification of CRL substrates that are specifically ubiquitylated at cellular membranes. We specifically focused on CRL3 complexes, members of a subclass of Cullin-RING ubiquitin ligases composed of the cullin scaffold Cul3 and a broad-complex, tramtrack, and bric-a-brac (BTB) protein as a substrate receptor subunit. Using this screen, we identified the ER-shaping protein Lunapark as a substrate of $CRL3^{KLHL12}$, a ubiquitin ligase complex containing the BTB protein kelch like family member 12 (KLHL12) as substrate receptor (Angers et al., 2006; Jin et al., 2012; Rondou et al., 2008). To investigate the biological function of Lunapark ubiquitylation, we have expressed a ubiquitylation-resistant Lunapark mutant in cultured cells as well as in zebrafish embryos. The results of these studies are herein presented.

RESULTS

A Proteomic Approach for the Identification of CRL Substrates that Are Ubiquitylated at Cellular Membranes

To systematically identify targets of the CRL3 ubiquitin ligase complexes that are ubiquitylated locally at cellular membranes, we performed affinity-purification and mass spectrometry analysis of CUL3 variants bearing, at their N termini, the lipid-modified motif (N11) of DCNL3, a co-E3 that contributes to the neddylation of CRL complexes at membranes (Keuss et al., 2016; Kurz et al., 2005, 2008; Meyer-Schaller et al., 2009; Monda et al., 2013; Scott et al., 2010, 2011). A schematic representation of the experimental design is shown in Figure 1A. The presence of the lipid-modified motif of DCNL3 at the N terminus of CUL3 is sufficient to stably recruit CUL3 to the plasma membrane and endomembranes (Figures 1B and S1) (Meyer-Schaller et al., 2009). To increase the stability of the CUL3-BTB protein-substrate complexes, the lipid-modified motif (N11) of DCNL3 was fused to two CUL3 mutants encoding the first 199 or 225 N-terminal amino acid residues (CUL3-N199 and CUL3-N225, respectively), which are unable to interact with RBX1. We expressed FLAG-tagged N11-CUL3-N199 or N11-CUL3-N225 as well as FLAG-tagged CUL3-N199 or CUL3-N225 without the lipid-modified motif (N11) in HEK293T cells and purified CUL3 immunoprecipitates, which were then analyzed by mass spectrometry. In addition to 51 BTB proteins and the RING-finger protein RBX1 (Figure 1C), which are known to directly bind CUL3 within the CRL3 complex, and various components of the CSN complex that play a regulatory role (not shown), we recovered numerous CRL3 candidate substrates. At least three of them (i.e., GBB1, GBB2, and ACLY) are known CRL3 targets (Bertocci et al., 2017; Brockmann et al., 2017; Zhang et al., 2016). Among the top 21 hits that were enriched in the pull-down of membrane-bound CUL3 (Figure 1D), 19 proteins are (1) described multi-pass or single-pass membrane proteins, (2) reported to contain putative transmembrane domains, or (3) found associated to the plasma membrane or membranes of various cellular organelles (The UniProt Consortium, 2017).

Lunapark Is Ubiquitylated by the $CRL3^{KLHL12}$ Ubiquitin Ligase Complex

Among the proteins found enriched in the affinity purification of membrane-bound CUL3 mutants (N11-CUL3-N199 or N11-CUL3-N225), we recovered Lunapark (Figure 1D; Tables S1 and S2), an evolutionarily conserved integral membrane protein involved in network formation of the ER (Chen et al., 2012, 2015; Goyal and Blackstone, 2013; Moriya et al., 2013; Shemesh et al., 2014; Wang et al., 2016). The interaction between N11-CUL3-N225 and endogenous Lunapark was confirmed by immunoprecipitation followed by immunoblotting (Figure 2A).

If Lunapark is a substrate of a CRL3 ubiquitin ligase, a specific BTB protein is expected to bind it and recruit it to CUL3 and the rest of the CRL3 complex. To identify the BTB protein that interacts with Lunapark, we immunopurified FLAG-tagged Lunapark from HEK293T cells. Mass spectrometry analysis of immunoprecipitated Lunapark identified the BTB protein KLHL12 as well as the CRL subunits RBX1 and CUL3 (Figure 2B) (Angers et al., 2006; Jin et al., 2012; Rondou et al., 2008). KLHL12 was the only BTB protein (out of the 169 BTB proteins encoded by the human genome) recovered in the affinity purification of FLAG-tagged Lunapark. The KLHL12-Lunapark interaction was confirmed by immunoprecipitation followed by immunoblotting (Figure 2C). Other BTB proteins, namely KLHL18, KCTD11, and SPOP/BTBD32, did not coimmunoprecipitate with endogenous Lunapark (Figure 2D). A complex with endogenous Lunapark and KLHL12 was also observed (Figure 2E). These results suggest that the $CRL3^{KLHL12}$ ubiquitin ligase mediates Lunapark ubiquitylation. To test this hypothesis, we examined whether ectopic expression of KLHL12 stimulates Lunapark

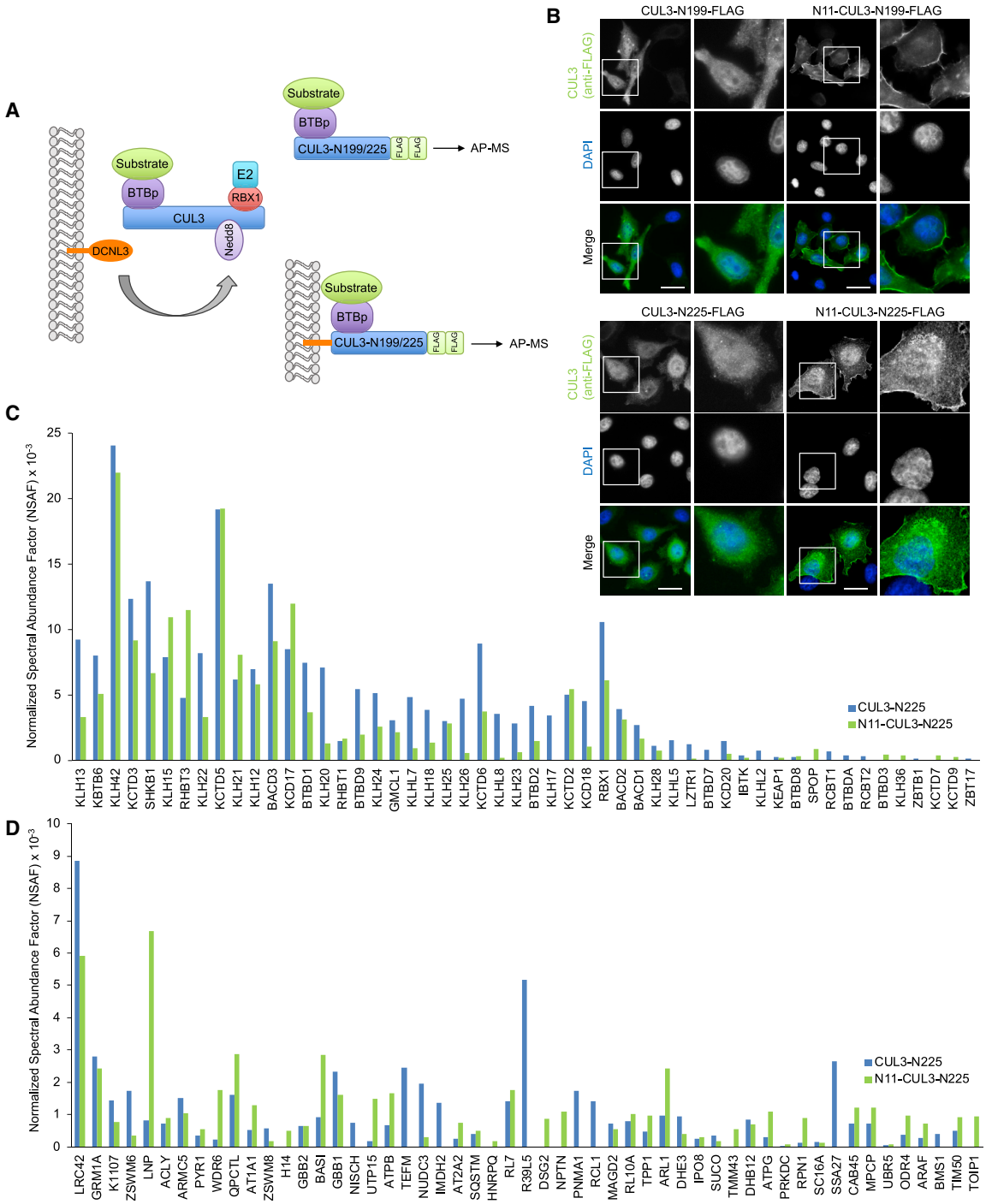

Figure 1. AP-MS-Based Screen to Identify CRL Substrates at Cellular Membranes

(A) Schematic representation of the experimental design aimed at identifying membrane associated CUL3 substrates.

(B) The indicated FLAG-tagged CUL3-N199 (top) and CUL3-N225 mutants (bottom) were expressed in HeLa cells. Cells were fixed and analyzed by immunofluorescence with an anti-FLAG antibody. DNA was stained with DAPI (blue). Bar indicates 20 μm.

(C and D) Graphical summary of CUL3 interactors, BTB proteins and RBX1 (C) and candidate substrates (D) that were recovered in the cytosolic/nuclear CUL3 pull-down (blue) or in the membrane-bound CUL3 pull-down (green). UniProt entry names are indicated on the X axes. Normalized spectral abundance factors (NSAFs) are shown on the Y axes.

See also Figure S1 and Tables S1 and S2.

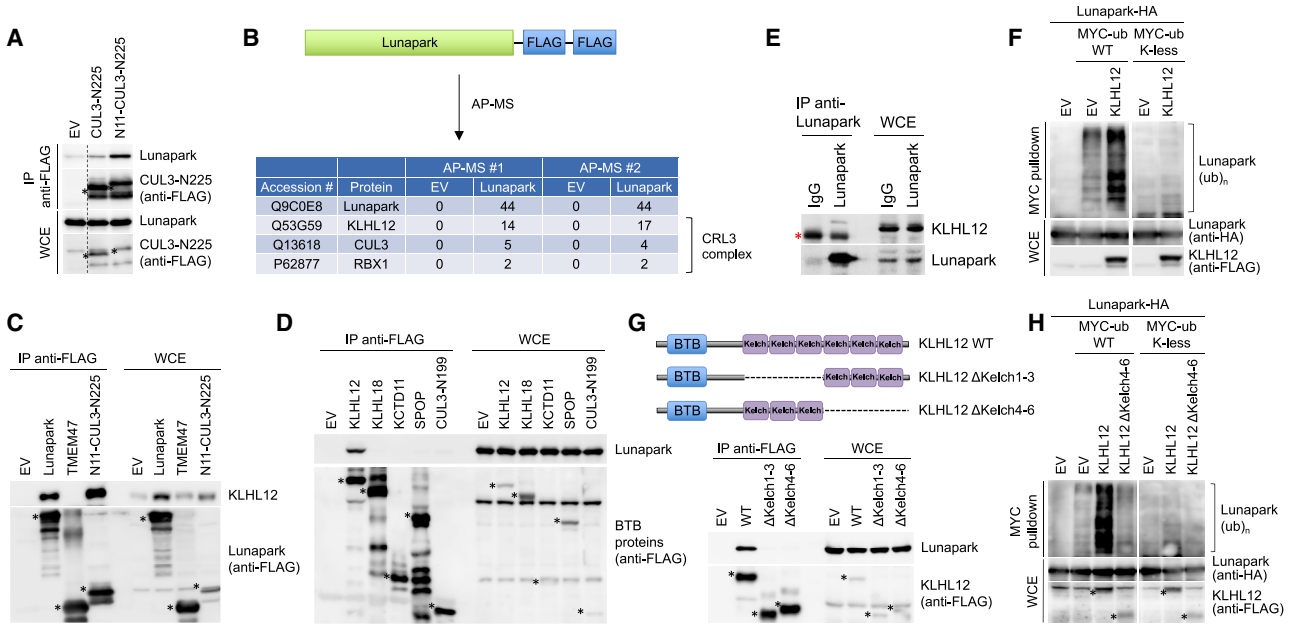

Figure 2. Lunapark Is a Substrate of the CRL3^{KLHL12} Ubiquitin Ligase

(A) HEK293T cells were transfected with an empty vector (EV) or the indicated FLAG-tagged CUL3 mutants. Whole-cell extracts (WCE) were immunoprecipitated (IP) with anti-FLAG resin and immunocomplexes were probed with antibodies to the indicated proteins. In all panels, black asterisks mark the FLAG-tagged proteins both in the IP and in the WCE.

(B) FLAG-tagged Lunapark was expressed in HEK293T cells. Cells were lysed and WCEs were subjected to immunoprecipitation using FLAG beads. Lunapark immunoprecipitates were then analyzed by mass spectrometry. The number of unique peptides identified by mass spectrometry in Lunapark and control immunopurifications is shown.

(C) HEK293T cells, transfected with FLAG-tagged Lunapark, the transmembrane protein TMEM47, and the membrane-bound N11-CUL3-N225 mutant, were lysed. WCE were immunoprecipitated (IP) with anti-FLAG resin and analyzed by immunoblotting.

(D) HEK293T cells, transfected with an EV or several FLAG-tagged BTB proteins, were lysed. WCE were used for FLAG immunoprecipitation and analyzed by immunoblotting. Note that the expressed CUL3 mutant does not contain the N-terminal lipid-modified motif and thus, as expected, does not interact with Lunapark.

(E) WCE from HEK293T cells were immunoprecipitated with an anti-Lunapark antibody. Lunapark immunocomplexes were then probed with antibodies to the indicated proteins. The red asterisk marks the IgG bands.

(F) HEK293T cells were transfected with HA-tagged Lunapark and MYC-tagged ubiquitin (wild-type [WT] or lysine-less [K-less]), with or without FLAG-tagged KLHL12. WCE were prepared in denaturing buffer and immunoprecipitated with an anti-MYC antibody. Immunoprecipitates were then immunoblotted to detect ubiquitylated Lunapark.

(G) Schematic representation of WT KLHL12 and two KLHL12 deletion mutants (top). HEK293T cells, transfected with an empty vector (EV), FLAG-tagged WT KLHL12 or the indicated KLHL12 mutants, were lysed. WCE were used for FLAG immunoprecipitations and probed for Lunapark binding by immunoblotting (bottom).

(H) As in (F), except that the KLHL12-ΔKelch4-6 mutant was also expressed.

See also Figure S2.

ubiquitylation in cultured cells. As shown in Figure 2F, Lunapark ubiquitylation is increased upon expression of KLHL12.

The BTB-Kelch proteins that form CRL3 ubiquitin ligase complexes contain an N-terminal BTB domain, which mediates their interaction with CUL3, and C-terminal Kelch repeats, which are required for substrate binding (Pintard et al., 2004). To test whether the Kelch repeats of KLHL12 are required for its interaction with Lunapark, we generated two KLHL12 mutants lacking either the first three or the last three Kelch repeats and assessed their ability to coimmunoprecipitate with endogenous Lunapark. As shown in Figure 2G, the two KLHL12-ΔKelch mutants do not interact with Lunapark further supporting a substrate-like interaction. Accordingly, the KLHL12-ΔKelch mutants are not able to stimulate Lunapark ubiquitylation in cells (Figures 2H and S2A). Taken together, these results suggest that Lunapark is a substrate of the CRL3^{KLHL12} ubiquitin ligase complex.

We then examined whether KLHL12-mediated ubiquitylation regulates Lunapark abundance. Treatment of cells with the NEDD8-activating enzyme inhibitor MLN4924, which blocks cullin neddylation and thus CRL activity, does not lead to Lunapark accumulation, but results in the accumulation of the CRL1 substrate β-catenin (Figure S2B). Likewise, proteasome inhibition by MG132 treatment does not have any effect on Lunapark abundance or turnover, whereas it leads to stabilization of the CRL1 substrates β-catenin and p27 (Figures S2B and S2C). Modulation of KLHL12 expression by RNA interference (Figure S2D) or overexpression (Figure S2E) does not result in any detectable change in the abundance of Lunapark. During

mitosis, Lunapark has been shown to be hyperphosphorylated (Wang et al., 2016). Because it has been suggested that phosphorylated Lunapark might be targeted for degradation in mitosis, we tested the effect of proteasome or CRL inhibition on the abundance of phosphorylated Lunapark. As shown in Figure S2F, Lunapark protein levels are not affected by either MG132 or MLN4924 treatment of mitotic cells. Taken together, these results demonstrate that Lunapark is ubiquitylated by the $CRL3^{KLHL12}$ ubiquitin ligase, and the $CRL3^{KLHL12}$-dependent ubiquitylation of Lunapark does not lead to its proteasomal degradation.

Analysis of the Minimal KLHL12-Binding Domain of Lunapark

Lunapark contains two N-terminal transmembrane domains (TMDs) that mediate its insertion into the outer leaflet of the ER membrane phospholipid bilayer, two TMD-flanking coiled coil regions, and a C-terminal zinc-finger motif (ZFM) that is essential for ER morphogenesis in yeast (Figure 3A). To map the KLHL12 binding motif in Lunapark, we generated multiple Lunapark deletion mutants and tested their interaction with endogenous KLHL12. We found that a proline-rich middle region (M, amino acids 138–246) in Lunapark is required for its binding to KLHL12 (Figure 3B). To narrow down the KLHL12 binding motif in Lunapark, we aligned the M region in different Lunapark vertebrate orthologs and identified three evolutionarily conserved regions, which we termed M1, M2, and M3 (Figure 3A). A series of pull-down experiments, in which the Lunapark ΔM1, ΔM2, and ΔM3 mutants were expressed in HEK293T cells and immunoprecipitated, narrowed the KLHL12 binding motif down to the M2 region of Lunapark (amino acids 202–210: SAPGGPPER) (Figure 3C). Accordingly, the KLHL12-mediated ubiquitylation of the Lunapark ΔM2 mutant was decreased when compared to the one of wild-type Lunapark (Figure 3D).

Further characterization of this 9-amino acid region by alanine-scanning mutagenesis demonstrated that mutation of the tri-amino-acid stretch SAP to AAA or GGP to AAA completely abolished Lunapark binding to KLHL12 (Figure 3E). Each of these tri-amino-acid stretches contains a proline forming a PXXP core, which is known to mediate the interaction to various domains that recognize proline-rich motifs (Kaneko et al., 2008). Therefore, we mutated both proline residues (i.e., Pro204 and Pro207) to alanine and determined the ability of the Lunapark(P204A/P207A) mutant to interact with KLHL12. As shown in Figure 3F, mutations of Pro204 and Pro207 rendered Lunapark unable to interact with KLHL12. Accordingly, Lunapark(P204A/P207A) is not ubiquitylated via KLHL12 in cultured cells (Figure 3G). Altogether, these data show that a Lunapark proline-rich domain centered on Pro204 and Pro207 mediates the binding of Lunapark to KLHL12 and its ubiquitylation.

As an additional approach to characterize the Lunapark-KLHL12 interaction, we employed immobilized synthetic peptides comprising the KLHL12-binding domain of Lunapark (aa 200–213). A Lunapark peptide containing Pro204 and Pro207 interacted with *in vitro* translated KLHL12, but not with a different BTB-Kelch protein (KLHL18), whereas the same peptide in which Pro204 and Pro207 were replaced by alanine did not associate at all, suggesting that Pro204 and Pro207 directly mediate the binding to KLHL12 (Figure 3H).

These results were further supported by computational molecular docking (Bordner and Abagyan, 2006; Lee et al., 2016; Neves et al., 2012). The peptide comprising the KLHL12-binding domain of Lunapark (aa 200–213) docks preferentially (large energy gap between lowest and next lowest conformation) to a groove on the molecular surface of KLHL12 with Pro204 and Pro207 forming the central loop of its interaction surface contacting the Kelch repeats of KLHL12 and Arg210 stabilizing the loop conformation intramolecularly (Figures 3I–3K). Replacing Pro204 and Pro207 with Ala and re-docking resulted in displacement of the peptide to a different, predicted conformation and location on the complex (Figure 3L) and a large reduction in the calculated energy of binding and the energy gap, indicating a more transient interaction (Figure 3M).

Lunapark Ubiquitylation Does Not Regulate ER Architecture and Dynamics

Next, we investigated the biological role of the KLHL12-dependent ubiquitylation of Lunapark. Because Lunapark is involved in the maintenance of the ER tubular network in mammalian cells (Chen et al., 2015), we examined whether inhibition of Lunapark ubiquitylation affects the architecture of the ER network and, in particular, the relative abundance of its two main morphological domains (i.e., ER sheets and tubules). To that end, we carried out live cell imaging analysis in U2OS cells expressing moderate levels of either GFP-tagged wild-type Lunapark or Lunapark(P204A/P207A) as well as the ER marker Sec61β fused to mCherry. As shown in Figures S3A and S3B, expression of the ubiquitylation-resistant Lunapark mutant did not affect the abundance of ER sheets and tubules. To further investigate a possible role of Lunapark ubiquitylation in the regulation of ER architecture, we generated Lunapark knockout U2OS cells by CRISPR-Cas9 genome editing. We then re-expressed in these cells moderate levels of either GFP-tagged wild-type Lunapark or Lunapark(P204A/P207A) (Figures S3C and S3D) as well as the ER marker Sec61β (fused to mCherry). Cells expressing GFP-tagged Lunapark(P204A/P207A) did not display any detectable change in ER architecture when compared to cells expressing wild-type Lunapark (Figures S3E and S3F). Moreover, both wild-type Lunapark and Lunapark(P204A/P207A) were detected as puncta with a diameter of 0.5–1 μm at three-way junctions (Figures S3 and S4) suggesting that the KLHL12-dependent ubiquitylation of Lunapark is not required for its localization to the ER three-way junctions. The same results were observed when the expression of KLHL12 was silenced by RNAi (not shown). We then analyzed the mobility of these junctions by marking the original position of Lunapark puncta and measuring the time it takes for each Lunapark puncta to move out of the circle. As shown in Figure S4, junctions with Lunapark(P204A/P207A) were as stable as junctions with wild-type Lunapark. Similarly, we did not observe differences in the percentage of merging and splitting junctions between cells containing Lunapark(P204A/P207A) and the ones containing wild-type Lunapark (Figure S4). Finally, inhibition of the KLHL12-dependent ubiquitylation of Lunapark does not affect Lunapark ability to form oligomers (Figure S5).

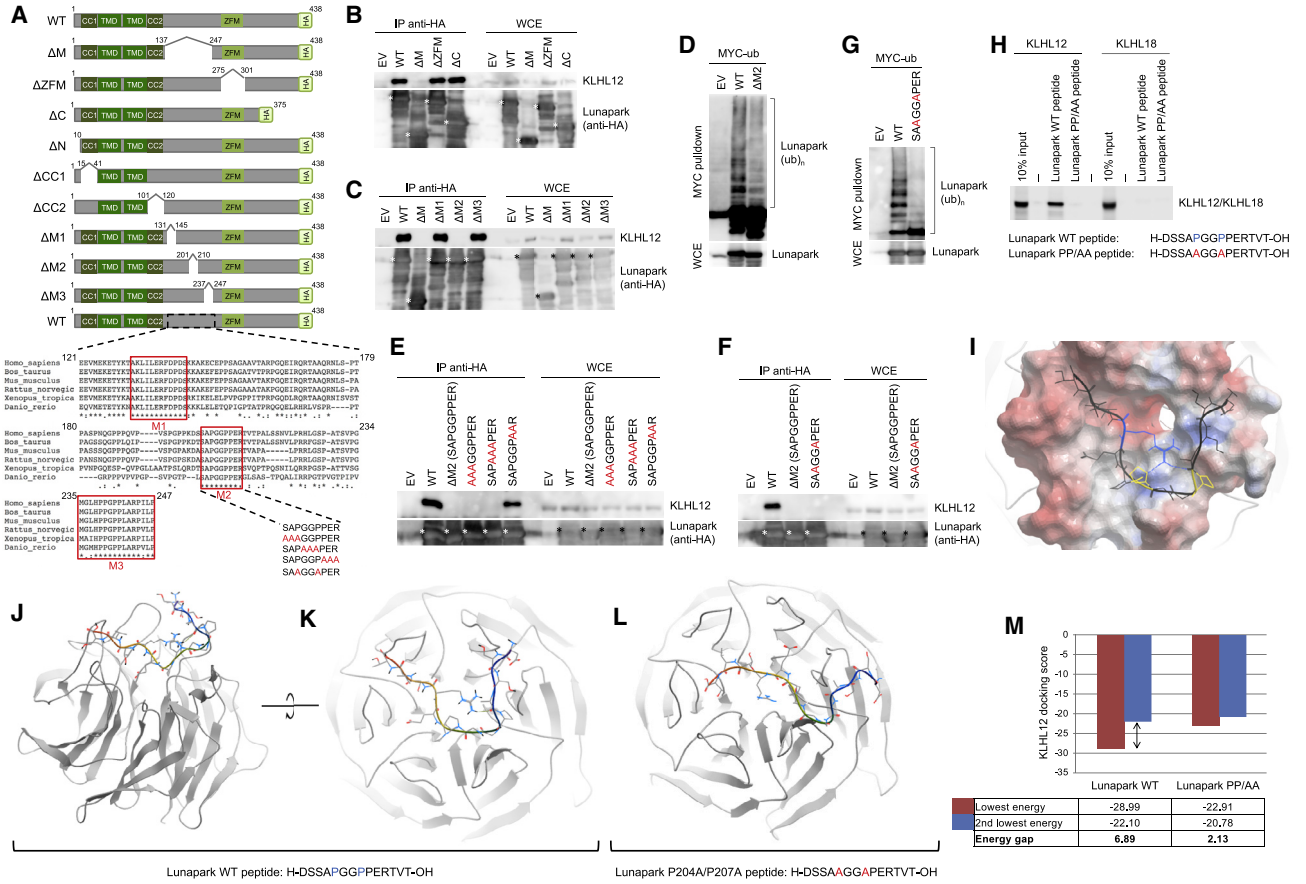

Figure 3. Identification of the KLHL12 Binding Site in Lunapark

(A) Top: schematic representation of WT Lunapark and the deletion mutants generated (TMD, transmembrane domain; CC, coiled-coil; ZFM, zinc-finger motif). Bottom: alignment of the Lunapark M (middle) region in vertebrate species. The evolutionarily conserved regions M1, M2, and M3 are boxed in red. Point mutants generated for alanine-scanning analysis are shown.

(B and C) HEK293T cells were transfected with an EV, HA-tagged WT Lunapark, or the indicated Lunapark mutants. WCEs were IP with anti-HA resin, and immunocomplexes were probed with antibodies to the indicated proteins. In all immunoblot panels, white and black asterisks mark the HA-tagged proteins in the IP and in the WCE.

(D) Ubiquitylation of Lunapark by KLHL12. HEK293T cells were transfected with HA-tagged Lunapark (WT or ΔM2 mutant), FLAG-tagged KLHL12, and MYC-tagged ubiquitin. WCE were prepared in denaturing buffer and identical aliquots were immunoprecipitated with antibodies directed against MYC. Immunoprecipitates were then immunoblotted to detect ubiquitylated Lunapark.

(E and F) As in (B) and (C).

(G) As in (D), except that the indicated Lunapark mutant was transfected instead of Lunapark ΔM2.

(H) *In vitro* binding between KLHL12 and a Lunapark peptide spanning Pro204 and Pro207. ^{35}S-KLHL12 and KLHL18 were transcribed/translated *in vitro* and incubated with beads coupled to a peptide spanning Pro204 and Pro207 or the same peptide in which Pro204 and Pro207 were replaced by alanine.

(I) Electrostatic surface rendering of KLHL12 with Lunapark WT peptide (black) with key residues highlighted: prolines whose substitution with alanines abrogates binding (yellow); arginine forming intramolecular bridge (blue).

(J) Ribbon representation of the Kelch domain of crystallized KLHL12 (PDB: 2VPJ; blue, N terminus; red, C terminus) and the predicted binding conformation of the Lunapark peptide.

(K and L) 90° anterior rotation of KLHL12 docking with Lunapark WT (K) or Lunapark(P204A/P207A) (L) peptide.

(M) Histogram of lowest energy conformation docking scores and energy gaps (Grigoryan et al., 2012) for Lunapark WT and the Lunapark(P204A/P207A) mutant peptides.

Lunapark Binds mTORC1 at ER Three-Way Junctions

The mass spectrometry analysis of endogenous proteins that copurified with FLAG-tagged Lunapark revealed the presence of peptides of mechanistic target of rapamycin (mTOR) and its cofactor mLST8 (Figure 4A). We confirmed the binding of ectopically expressed Lunapark to endogenous mTOR and mLST8 by coimmunoprecipitation (Figure 4B). A complex with endogenous Lunapark and mTOR was also detected by either immunoprecipitating Lunapark (Figure 4C) or mTOR (Figure 4D). However, neither Raptor nor Rictor, complex-specific subunits of mTORC1 and mTORC2 respectively, were detected by immunoblotting or mass spectrometry in the Lunapark

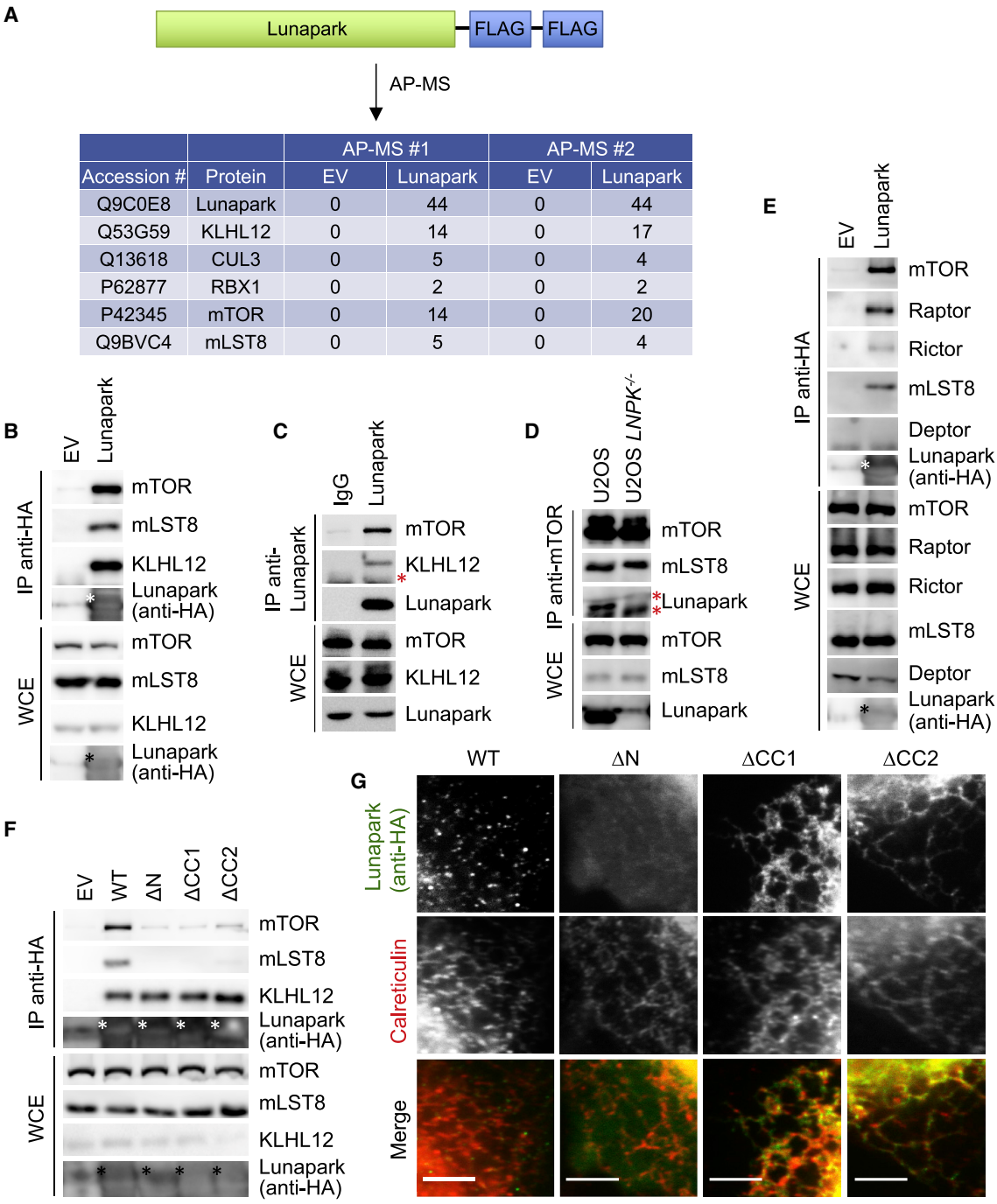

		AP-MS #1		AP-MS #2	
Accession #	Protein	EV	Lunapark	EV	Lunapark
Q9C0E8	Lunapark	0	44	0	44
Q53G59	KLHL12	0	14	0	17
Q13618	CUL3	0	5	0	4
P62877	RBX1	0	2	0	2
P42345	mTOR	0	14	0	20
Q9BVC4	mLST8	0	5	0	4

Figure 4. Lunapark Binds mTORC1 at ER Three-Way Junctions

(A) FLAG-tagged Lunapark was expressed in HEK293T cells and immunoprecipitated. Immunocomplexes were then analyzed by mass spectrometry. The number of unique peptides identified by mass spectrometry in Lunapark and control immunopurifications is shown.

(B) HEK293T cells were transfected with an EV or HA-tagged Lunapark. WCEs were IP with anti-HA resin, and immunocomplexes were probed with antibodies to the indicated proteins. In all immunoblot panels, white and black asterisks mark the HA-tagged proteins in the IP and in the WCE.

(C) WCE from HEK293T cells were immunoprecipitated with an anti-Lunapark antibody. Lunapark immunocomplexes were then probed with antibodies to the indicated proteins. The red asterisk marks unspecific bands.

(D) WCE from parental or *LNPK*$^{-/-}$ U2OS cells were immunoprecipitated with an anti-mTOR antibody. mTOR immunocomplexes were then probed with antibodies to the indicated proteins. The red asterisks mark unspecific bands.

(legend continued on next page)

immunoprecipitation. As NP40 (used in the affinity purification-mass spectrometry [AP-MS] shown in Figure 4A) and Triton X-100 (used in the pull-down shown in Figures 4B–4D) are known to disrupt the Raptor-mTOR and Rictor-mTOR interactions (Hara et al., 2002; Kim et al., 2002; Sarbassov et al., 2004), we immunoprecipitated Lunapark in the presence of the reversible crosslinker dithiobis(succinimidyl propionate) (DSP) which was shown to preserve both the Raptor-mTOR and Rictor-mTOR interactions (Hara et al., 2002; Kim et al., 2002; Sarbassov et al., 2004). Using these experimental conditions, we found that Raptor is also part of the Lunapark-mTOR-mLST8 complex that was pulled down from cell lysates (Figure 4E).

Next, we examined the ability of various Lunapark mutants to coimmunoprecipitate with endogenous mTOR and mLST8. Two Lunapark mutants that are still localized to the ER but do not concentrate at the ER three-way junctions due to the deletion of either of the two coiled-coil regions (CC1 or CC2) adjacent to the transmembrane motifs (Figure 3A) (Wang et al., 2016; Zhao et al., 2016) do not interact with mTOR and mLST8 (Figure 4F and 4G). Similarly, a Lunapark mutant that lacks the N-terminal myristoylated Gly2, and consequently is not localized to the ER, is unable to coimmunoprecipitate with mTOR and mLST8 (Figures 3A, 4F, and 4G). Taken together, these results indicate that the localization of Lunapark to ER three-way junctions is required for its binding to mTORC1.

mTORC1-Positive Lysosomes and Late Endosomes Form Contact Sites with Lunapark-Containing Three-Way Junctions

We then characterized the Lunapark-mTOR interaction in cultured cells. First, we detected, by *in situ* proximity ligation assay (PLA), the interaction between endogenous mTOR and Lunapark stably re-expressed (at physiological levels) in *LNPK*$^{-/-}$ U2OS cells generated by CRISPR-Cas9 technology (Figures 5A–5C and S3C). No signal was observed when only one antibody was used in these cells or when both antibodies were used in *LNPK*$^{-/-}$ U2OS cells. Notably, *in situ* PLA carried out in cells expressing GFP-Sec61β showed PLA puncta (marking the mTOR/Lunapark interaction) at ER three-way junctions (Figure 5D). Second, we examined the localization of Raptor, the complex-specific subunit of mTORC1, and Lunapark by live confocal fluorescence microscopy. U2OS cells were transfected with mCherry-Raptor and GFP-Lunapark and imaged by live confocal fluorescence microscopy. As shown in Figure 5E, Raptor-positive puncta were detected adjacent to Lunapark-positive puncta at the cell periphery where both signals can be well resolved.

The recruitment of mTORC1 to the membrane of lysosomes and late endosomes (LyLEs) via the Rag guanosine triphosphatases (GTPases) in response to amino acids is an obligate step in the activation of mTORC1 (Saxton and Sabatini, 2017). Once at the LyLE surface, mTORC1 interacts with GTP-bound Rheb, which unlocks the kinase activity of mTORC1 triggering phosphorylation of its substrates. Because active mTORC1 is localized to the LyLE membrane, we tested whether ER three-way junctions (where Lunapark resides) and LyLEs (where mTORC1 is recruited and activated) make contact. To visualize the ER and LyLEs, U2OS cells were co-transfected with mCherry-Sec61β (an ER marker) and GFP-LAMP1 (a LyLE marker). ER and LyLEs were then imaged by live confocal fluorescence microscopy at the cell periphery where both organelles can be well resolved (Figure 5F). LyLEs were found to be in close proximity to, or in contact with, tubular regions of the ER and associated with ER three-way junctions. This association was dynamic and variable as LyLEs transiently made contact and overlap with ER three-way junctions and tubules before dissociating and contacting the ER elsewhere. Examples of LyLE-ER contacts are shown in Figure 5F. We could distinguish between LAMP1-positive structures that overlap with ER three-way junctions (top), are in apposition with three-way junctions (middle), or partly overlap (bottom). Accordingly, when we imaged cells expressing mCherry-LAMP1 and GFP-Lunapark, we observed Lunapark-positive puncta contacting LAMP1-positive structures (Figures 5G and 5H). Finally, live cell imaging analysis of triple-labeled U2OS cells expressing GFP-Lunapark, BFP-KDEL (ER marker), and mCherry-LAMP1 (lysosome marker) confirmed that Lunapark-positive ER three-way junctions and LyLEs make contact (Figure S6). Of note, we observed LyLEs associating with ER regions that contain Lunapark (mostly at the ER three-way junctions) as well as LyLEs associating with ER regions that do not contain Lunapark (not at ER three-way junctions) in agreement with previous studies (Rowland et al., 2014).

Inhibition of Lunapark Ubiquitylation Affects Lysosomal Recruitment of mTORC1

Next, we assessed whether the KLHL12-dependent ubiquitylation of Lunapark affects mTORC1 translocation to the lysosomal membrane. We employed Lunapark-knockout U2OS cells (generated by CRISPR-Cas9 technology) transduced with lentiviruses expressing physiological levels of either HA-tagged wild-type Lunapark or the Lunapark(P204A/P207A) mutant that is unable to interact with KLHL12 and be ubiquitylated (Figures 6A and S3D). These cells were stimulated with amino acids and immunostained for endogenous mTOR and the lysosome marker LAMP2 (Sancak et al., 2010). In cells expressing wild-type Lunapark, mTOR colocalized with LAMP2 in the presence, but not in the absence of amino acids where mTOR was dispersed throughout the cytoplasm (Figure 6B-C). Cells expressing Lunapark(P204A/P207A) displayed increased amino acid-induced colocalization of mTOR with the lysosomal surface (LAMP2) when compared with control cells.

As the translocation of mTORC1 to the lysosomal membrane triggers its activation, we analyzed whether the KLHL12-mediated ubiquitylation of Lunapark affects mTORC1 signaling activity. Compared to nutrient-stimulated cells expressing wild-type

(E) As in (B) except that the reversible crosslinker dithiobis(succinimidyl propionate) (DSP) was used.
(F) As in (B) except that the indicated Lunapark mutants (described in Figure 3A) were also expressed.
(G) U2OS cells expressing HA-tagged WT Lunapark or the indicated Lunapark mutants (as in E) were fixed and immunostained for HA (green) and the ER marker calreticulin (red). Scale bar indicates 5 μm.

CellPress
OPEN ACCESS

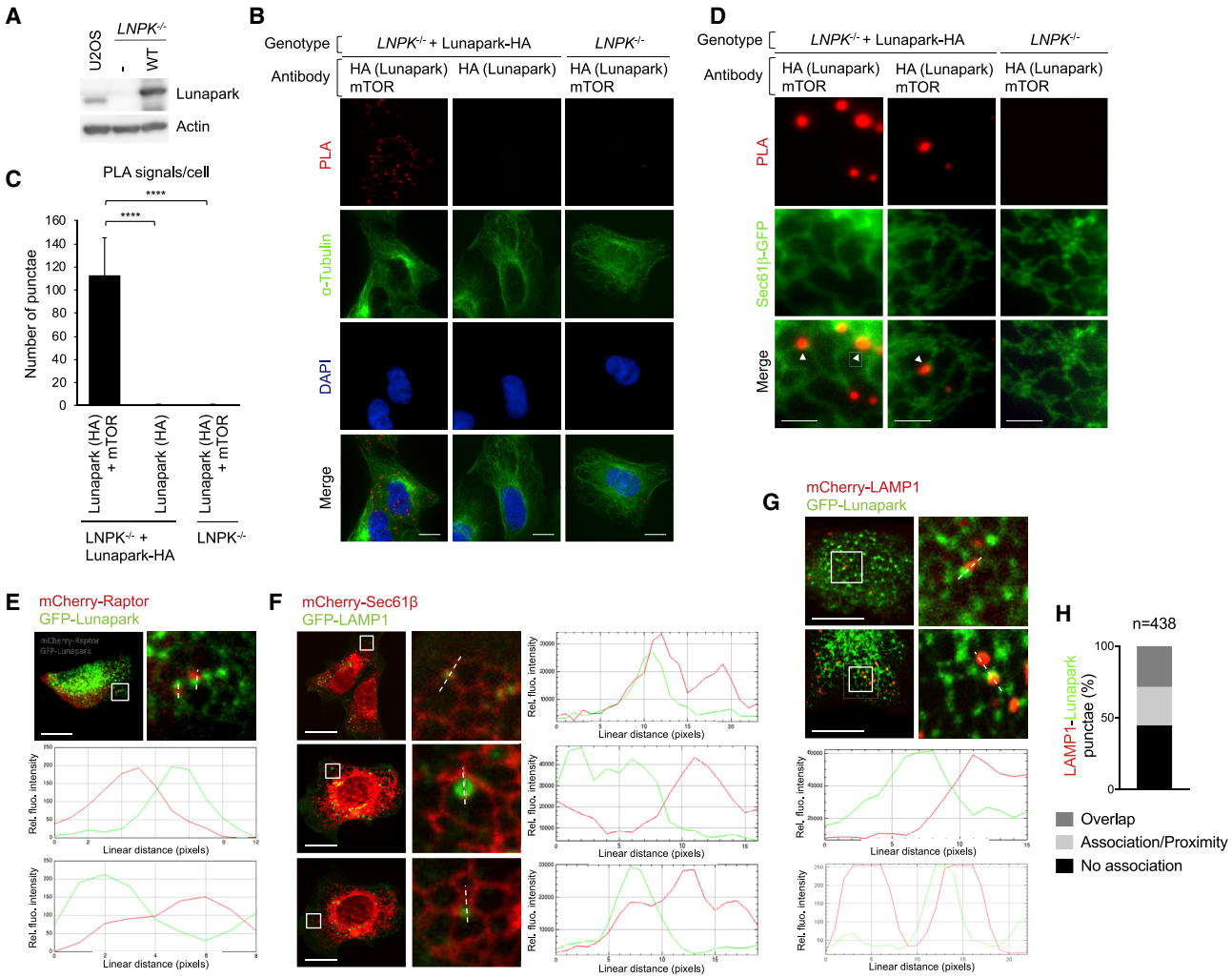

Figure 5. mTORC1-Positive LyLEs Form Contact Sites with Lunapark-Containing Three-Way Junctions

(A) Parental, *LNPK*$^{-/-}$, or *LNPK*$^{-/-}$ U2OS cells re-expressing HA-tagged WT Lunapark were lysed. Whole cell extracts were analyzed by immunoblotting with antibodies specific for the indicated proteins.

(B) *In situ* PLA of *LNPK*$^{-/-}$ U2OS cells or *LNPK*$^{-/-}$ U2OS cells re-expressing HA-tagged Lunapark probed with the indicated antibodies. Cells were counterstained with an anti-α-tubulin-FITC-conjugated antibody. The cell genotypes and the antibodies utilized are indicated on top. Scale bar indicates 10 μm.

(C) Quantification of (B). p values <0.0001 are indicated with four asterisks.

(D) As in (B), except that cells were transfected with GFP-Sec61β to visualize the ER network and not counterstained. Left and middle panels show two *LNPK*$^{-/-}$ + Lunapark-HA cells with PLA puncta localized to three-way junctions (pointed by white triangles, both anti-mTOR and anti-HA antibodies are employed). The right panels show a *LNPK*$^{-/-}$ cell stained with both antibodies (anti-mTOR and anti-HA). Scale bar indicates 2 μm.

(E) Live cell epifluorescence images and relative magnification insets of U2OS cells expressing mCherry-Raptor and GFP-Lunapark. Scale bar indicates 10 μm. Corresponding line-scan graphs of the relative fluorescence intensities of GFP and mCherry along the line indicated in the images are shown (bottom). The top line-scan graph corresponds to the left dotted line whereas the bottom line-scan graph corresponds to the right dotted line.

(F) As in (E), except that U2OS cells express mCherry-Sec61β and GFP-LAMP1. LAMP1 positive structures that overlap with ER three-way junctions (top), are in apposition with three-way junctions (middle) or partly overlap (bottom) are shown.

(G) As in (E), except that U2OS cells express mCherry-LAMP1 and GFP-Lunapark.

(H) Percentage of mCherry-LAMP1 puncta that show overlap, association/proximity, or no association with GFP-Lunapark (n = 438).

See also Figures S3 and S6

Lunapark, nutrient-stimulated cells expressing Lunapark(P204A/P207A) displayed increased degree and duration of mTORC1 activation as measured by phosphorylation of the mTORC1 substrate S6-kinase (Figures 6D and 6E). Of note, the pattern of S6K phosphorylation looks alike in parental U2OS cells and LNPK$^{-/-}$ U2OS cells reexpressing wild-type Lunapark indicating that the increased mTORC1 activity observed in LNPK$^{-/-}$ U2OS cells re-expressing Lunapark(P204A/P207A) is not due to its overexpression. To rule out that the observed phenotype may result from the expression of a non-functional Lunapark protein caused by the Pro204/207 substitution that could impair protein structure and function, we prevented Lunapark ubiquitylation in U2OS cells

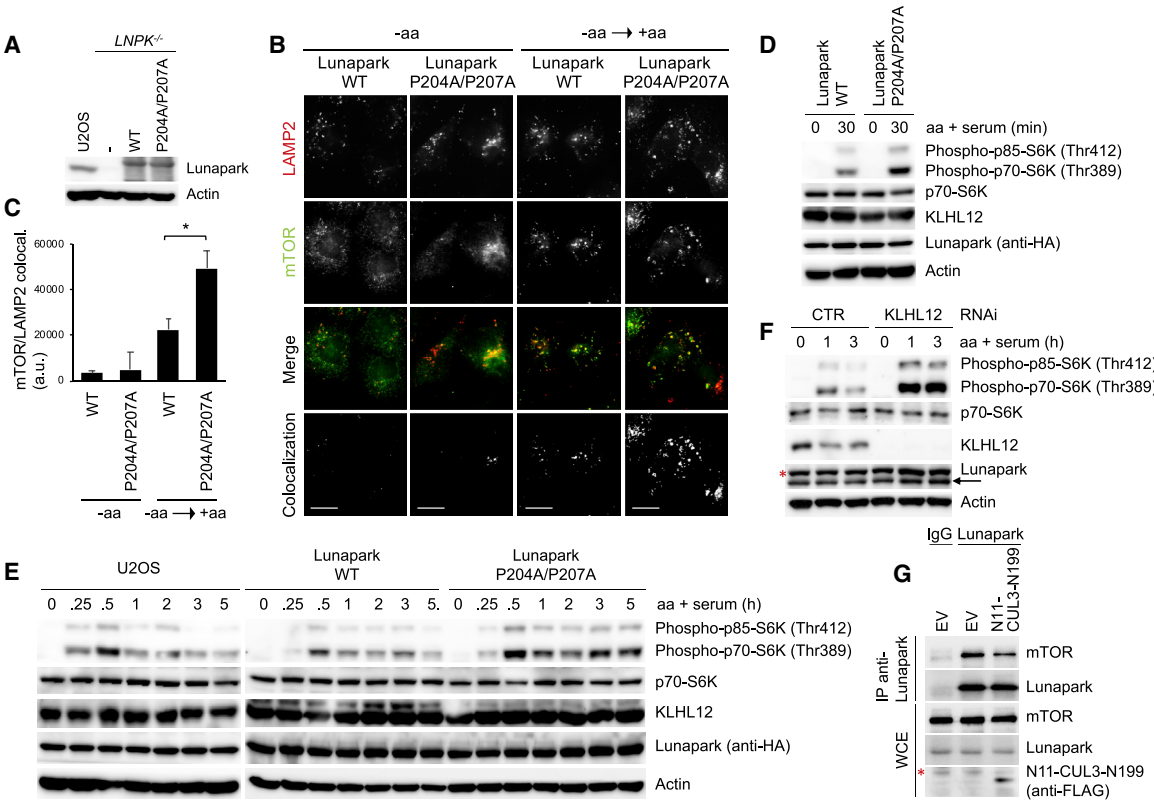

Figure 6. KLHL12-Dependent Ubiquitylation of Lunapark Limits mTOR Targeting to the Lysosomes and mTORC1 Activation

(A) Parental, *LNPK*$^{-/-}$, or *LNPK*$^{-/-}$ U2OS cells re-expressing WT Lunapark or Lunapark(P204A/P207A) were lysed. WCEs were then analyzed by immunoblotting.

(B) *LNPK*$^{-/-}$ or *LNPK*$^{-/-}$ U2OS cells re-expressing (by lentiviral transduction) either WT Lunapark or Lunapark(P204A/P207A) were starved of amino acids for 50 min and then re-stimulated for 10 min. Cells were then fixed and immunostained for endogenous mTOR (green) and the lysosomal marker protein LAMP2 (red). Colocalization panels show overlapping LAMP2 and mTOR signals. Scale bar indicates 10 μm.

(C) Quantification of mTOR/LAMP2 colocalization shown in (B). Three independent experiments were performed (n = 100 for each condition). Mean ± SD. *$p \leq 0.01$.

(D) *LNPK*$^{-/-}$ cells re-expressing WT Lunapark or Lunapark(P204A/P207A) were starved of amino acids for 50 min and then re-stimulated for the indicated times. Cells were collected, lysed, and analyzed by immunoblotting.

(E) As in (D), except that also parental U2OS cells were also analyzed.

(F) U2OS cells were transfected with either an siRNA targeting KLHL12 or a control siRNA and then treated as in (D). The red asterisk marks an unspecific band.

(G) HEK293T cells were transfected with an EV or N11-CUL3-N199 and lysed. WCE were used for Lunapark immunoprecipitation (employing an anti-Lunapark antibody) and analyzed by immunoblotting. As additional negative control, cells transfected with an EV were mocked immunoprecipitated using control IgGs. The red asterisk marks an unspecific band.

See also Figures S3, S4, S5, S6, and S7.

by silencing KLHL12 expression. The phosphorylation of S6-kinase was increased in KLHL12 knockdown cells when compared with the one in cells transfected with control small interfering RNA (siRNA) (Figure 6F) indicating that mTORC1 hyperactivation results from inhibition of the KLHL12-dependent ubiquitylation of Lunapark. Moreover, the KLHL12-mediated ubiquitylation of Lunapark limits mTORC1 activation also in non-transformed cells. Indeed, as shown in Figures S7A and S7B, the knockdown of KLHL12 as well as the expression of the ubiquitylation-resistant Lunapark mutant in hTERT-RPE cells results in increased degree and duration of mTORC1 activation.

We then tested the effect of blocking Lunapark ubiquitylation in response to amino acid deprivation. The rationale behind this experiment was to examine whether cells in which the KLHL12-mediated ubiquitylation of Lunapark is blocked are insensitive to stimuli or conditions that inactivate mTORC1. As shown in Figures S7C and S7D, cells expressing Lunapark(P204A/P207A) display the same kinetics of mTOR inactivation when compared to cells expressing wild-type Lunapark as judged by S6K dephosphorylation in response to nutrient withdrawal. The same results were obtained when we blocked the activity of mTORC1 by treating cells with rapamycin (Figure S7E).

Inhibition of Lunapark Ubiquitylation Results in Neurodevelopmental Defects

To investigate the role of the KLHL12-dependent ubiquitylation of Lunapark in normal growth and development, one-cell stage zebrafish embryos were microinjected with mRNA encoding

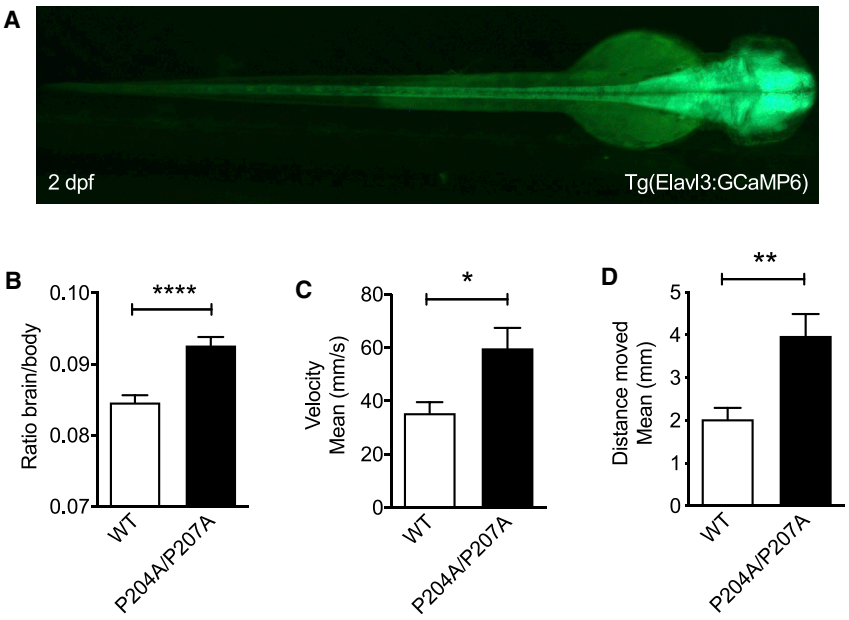

Figure 7. Expression of the Ubiquitylation-Resistant Lunapark Mutant in Zebrafish Results in Megalencephaly and Sensitizes Zebrafish to Pentylenetetrazole (PTZ) Treatment

(A) Dorsal view of a 2 dpf Tg(Elavl3:GCaMP6) embryo employed for the phenotypic analysis described in (B).

(B) Tg(Elavl3:GCaMP6) zebrafish embryos were injected with mRNA encoding WT Lunapark or Lunapark(P204A/P207A). The brain size of 2 dpf microinjected embryos was measured and normalized against the body length. Mean ± SEM. ****$p < 0.0001$ (Student's t test).

(C and D) Zebrafish embryos were injected as in (B). Four dpf injected larvae were placed in wells of a flat-bottom plate. Locomotion analysis was carried out as described in the STAR Methods. The graphs show velocity (C) and distance covered (D) by the injected larvae. Mean ± SEM. *$p < 0.05$, **$p < 0.01$ (Student's t test).

wild-type Lunapark or Lunapark(P204A/P207A). No significant phenotypic alterations in the head, heart, swim bladder, eye, tail, and fin were identified in injected zebrafish until 5 days post-fertilization (dpf). However, larvae expressing Lunapark(P204A/P207A) displayed larger brains when compared to sibling larvae expressing wild-type Lunapark (Figures 7A and 7B). Interestingly, mTOR signaling has been shown to be critical in brain development. Loss of function mutations in the tuberous sclerosis complex TSC1 or TSC2 genes, which lead to dysregulated mTOR activity, are associated with brain lesions, epilepsy, cognitive impairment, and autism (Luarte et al., 2018; Switon et al., 2017). Moreover, mTOR hyperactivation resulting from inhibition of TSC2 or Depdc5 expression in zebrafish has been associated with altered locomotion activity (de Calbiac et al., 2018; Scheldeman et al., 2017). Therefore, we tested whether blocking Lunapark ubiquitylation affects locomotion activity in zebrafish. Four dpf larvae injected with wild-type Lunapark or Lunapark(P204A/P207A) mRNAs were placed into individual wells of a 24-well plate and acclimated to a recording chamber. Locomotor analysis performed in basal condition did not revealed significant differences in activity between the two samples (data not shown). However, Lunapark(P204A/P207A)-expressing larvae treated with low doses of the CNS proconvulsant pentylenetetrazole (PTZ) displayed increased locomotor activity when compared to larvae injected with wild-type Lunapark (Figures 7C and 7D). Taken together, our results show that inhibition of Lunapark ubiquitylation in zebrafish results in megalencephaly and increased sensitivity to chemical compounds that induce epilepsy.

DISCUSSION

Our biochemical data indicate that the interaction of Lunapark with KLHL12 is mediated by the Kelch repeats of KLHL12 and a Lunapark proline-rich domain centered on Pro204 and Pro207. These results are supported by computational molecular docking, which indicates that the peptide containing Pro204 and Pro207 is also structurally and energetically complementary to the KLHL12 binding groove and is displaced by mutation of the prolines. Currently we do not know how the KLHL12-Lunapark interaction is regulated, however, we believe that proline hydroxylation might control Lunapark binding to KLHL12. Indeed, we retrieved Lunapark peptides harboring hydroxylated Pro204 in our mass spectrometry data and found that Pro204, which is essential for Lunapark binding to KLHL12, lies within a region matching the canonical X-Pro-Gly recognition sequence of prolyl 4-hydroxylases (P4Hs), enzymes that catalyze proline hydroxylation, yielding (2S,4R)-4-hydroxyproline (Hyp) (Gorres and Raines, 2010; Qi et al., 2008). P4Hs are $\alpha 2\beta 2$ tetramers in which the α-subunits contain enzymatic activity and a substrate-binding domain, while the β-subunits function as a protein disulfide isomerase (PDI) that anchors the enzyme to the ER. For the prolyl hydroxylation reaction P4Hs require α-ketoglutarate (αKG), which acts as the rate limiting electron donor under normoxic conditions (Gorres and Raines, 2010; Qi et al., 2008). αKG is the product of the deamination of glutamine, a potent mTORC1 activator. Indeed during glutaminolysis, glutaminases catalyze the conversion of glutamine into glutamate, which is then deamined to αKG (Durán et al., 2013; Jewell et al., 2015; Villar et al., 2015). The conversion of glutamate to αKG depends on the allosteric activation of glutamate dehydrogenase (GDH) by leucine and the metabolism of other amino acids, such as arginine, proline, and histidine, also results in αKG production. Thus, the KLHL12-mediated ubiquitylation of Lunapark might be part of a feedback mechanism in which amino acid abundance increases αKG production thus promoting the P4H-dependent hydroxylation of Lunapark. In turn, hydroxylation of Pro204 would stimulate Lunapark interaction with KLHL12 and

Lunapark ubiquitylation, preventing nutrient-stimulated hyper-accumulation of mTORC1 on the lysosomal membrane and de-regulated mTORC1 signaling.

How the KLHL12-dependent ubiquitylation of Lunapark limits the activation of mTORC1 in response to amino acids is not known. Our results show that inhibition of Lunapark ubiquitylation decreases its interaction with mTOR (Figure 6G). Interestingly, it has been recently shown that when amino acids are abundant, mTORC1 is only transiently associated with the lysosomal membrane as it undergoes dynamic binding and release cycles at the lysosomal surface (Lawrence et al., 2018). This mechanism prevents mTORC1 hyperactivation by reducing the amount of time during which mTORC1 is in direct contact with its activator Rheb at the lysosomal membrane. One possibility that needs to be tested is that Lunapark ubiquitylation mediated by KLHL12 could regulate the accumulation of mTORC1 to the lysosomal membrane by affecting its spatial cycling.

Our data demonstrate that inhibition of Lunapark ubiquitylation results in neurodevelopmental defects in *D. rerio*. Although Lunapark is ubiquitously expressed, it is present at high levels in the CNS of mice and chickens during embryo development and is involved in synaptic vesicle transport in *C. elegans* neuronal structures (Ghila and Gomez, 2008). Furthermore, Lunapark expression was observed throughout brain development in both mice and humans as well as in differentiating neural precursor cells (Breuss et al., 2018). Recently, homozygous mutations in the gene encoding Lunapark have been described in three children with a recessive neurodevelopmental syndrome characterized by intellectual disability, psychomotor developmental delay, defects in social interactions, hyperactivity, inattention, and epilepsy (Breuss et al., 2018). Interestingly, hyperactivation of mTORC1 signaling observed in tuberous sclerosis complex patients results in epilepsy, neurodevelopmental delays, behavioral problems including attention deficit hyperactivity disorder, and autism spectrum disorder (Luarte et al., 2018; Switon et al., 2017). Moreover, mutations in any of the three components (DEPDC5, NPRL2, and NPRL3) of the GATOR1 complex, which inhibits mTORC1 signaling by acting as a GAP for RagA/B, results in epilepsy (Marsan and Baulac, 2018).

Although proper ER morphology is key in many cellular processes and tissues, axons that require a highly elongated ER polygonal network are more sensitive to perturbations of the ER architecture (Luarte et al., 2018). Indeed, the axonal ER network is essential for vesicular transport from the soma to the axon growth cone, lipid, and cholesterol synthesis as well as their trafficking to the synapses, and it is crucial for axonal Ca^{2+} dynamics. Accordingly, mTOR has been shown to be essential for neuron development, specifically dendritogenesis, neuronal physiology, axon guidance, and axonogenesis. An assessment of the role of Lunapark ubiquitylation in neurons and its potential implication in neurodegeneration should be warranted.

STAR★METHODS

Detailed methods are provided in the online version of this paper and include the following:

SUPPLEMENTAL INFORMATION

Supplemental Information can be found online at https://doi.org/10.1016/j.celrep.2020.107664.

ACKNOWLEDGMENTS

The authors thank M. Rossi, C. Rabouille, and M. Perduca for helpful comments and discussion, the aquarium team of the Interdepartmental Centre for Experimental Research (C.I.R.S.A.L.) (University of Verona) for zebrafish husbandry, L. Di Marcotullio for reagents, and L.M. Young, C. Valdes Quezada, Z. Lei, R. Magliozzi, M. Marogna, and E. Cadoria for contributions. This work was funded by grants from the Dutch Cancer Society (KWF) and Fondazione Cariverona to D.G.

AUTHOR CONTRIBUTIONS

Conceptualization, L.Y., A.L., A.V., T.C., and D.G.; Methodology, L.Y., A.L., M.G., S.A., E.N., C.T., J.O.O., and T.Y.L.; Investigation, L.Y., A.L., M.G., S.A., E.N., C.T., J.O.O., and T.Y.L.; Writing, D.G.; Funding Acquisition, D.G.; Resources, A.V., T.C., A.J.R.H., and D.G.; Supervision, D.G.

DECLARATION OF INTERESTS

The authors declare no competing interests.

Received: March 12, 2019
Revised: January 16, 2020
Accepted: April 28, 2020
Published: May 19, 2020

REFERENCES

Angers, S., Thorpe, C.J., Biechele, T.L., Goldenberg, S.J., Zheng, N., MacCoss, M.J., and Moon, R.T. (2006). The KLHL12-Cullin-3 ubiquitin ligase negatively regulates the Wnt-beta-catenin pathway by targeting Dishevelled for degradation. Nat. Cell Biol. *8*, 348–357.

Astone, M., Lai, J.K.H., Dupont, S., Stainier, D.Y.R., Argenton, F., and Vettori, A. (2018). Zebrafish mutants and TEAD reporters reveal essential functions for Yap and Taz in posterior cardinal vein development. Sci. Rep. *8*, 10189.

Bertocci, B., Lecoeuche, D., Sterlin, D., Kühn, J., Gaillard, B., De Smet, A., Lembo, F., Bole-Feysot, C., Cagnard, N., Fadeev, T., et al. (2017). Klhl6 Deficiency Impairs Transitional B Cell Survival and Differentiation. J. Immunol. *199*, 2408–2420.

Bordner, A.J., and Abagyan, R. (2006). Ab initio prediction of peptide-MHC binding geometry for diverse class I MHC allotypes. Proteins *63*, 512–526.

Breuss, M.W., Nguyen, A., Song, Q., Nguyen, T., Stanley, V., James, K.N., Musaev, D., Chai, G., Wirth, S.A., Anzenberg, P., et al. (2018). Mutations in LNPK, Encoding the Endoplasmic Reticulum Junction Stabilizer Lunapark, Cause a Recessive Neurodevelopmental Syndrome. Am. J. Hum. Genet. *103*, 296–304.

Brockmann, M., Blomen, V.A., Nieuwenhuis, J., Stickel, E., Raaben, M., Bleijerveld, O.B., Altelaar, A.F.M., Jae, L.T., and Brummelkamp, T.R. (2017). Genetic wiring maps of single-cell protein states reveal an off-switch for GPCR signalling. Nature *546*, 307–311.

Canning, P., Cooper, C.D., Krojer, T., Murray, J.W., Pike, A.C., Chaikuad, A., Keates, T., Thangaratnarajah, C., Hojzan, V., Ayinampudi, V., et al. (2013). Structural basis for Cul3 protein assembly with the BTB-Kelch family of E3 ubiquitin ligases. J. Biol. Chem. *288*, 7803–7814.

Chen, S., Novick, P., and Ferro-Novick, S. (2012). ER network formation requires a balance of the dynamin-like GTPase Sey1p and the Lunapark family member Lnp1p. Nat. Cell Biol. *14*, 707–716.

Chen, S., Novick, P., and Ferro-Novick, S. (2013). ER structure and function. Curr. Opin. Cell Biol. *25*, 428–433.

Chen, S., Desai, T., McNew, J.A., Gerard, P., Novick, P.J., and Ferro-Novick, S. (2015). Lunapark stabilizes nascent three-way junctions in the endoplasmic reticulum. Proc. Natl. Acad. Sci. USA *112*, 418–423.

de Calbiac, H., Dabacan, A., Marsan, E., Tostivint, H., Devienne, G., Ishida, S., Leguern, E., Baulac, S., Muresan, R.C., Kabashi, E., and Ciura, S. (2018). Depdc5 knockdown causes mTOR-dependent motor hyperactivity in zebrafish. Ann. Clin. Transl. Neurol. *5*, 510–523.

Durán, R.V., MacKenzie, E.D., Boulahbel, H., Frezza, C., Heiserich, L., Tardito, S., Bussolati, O., Rocha, S., Hall, M.N., and Gottlieb, E. (2013). HIF-independent role of prolyl hydroxylases in the cellular response to amino acids. Oncogene *32*, 4549–4556.

Friedman, J.R., and Voeltz, G.K. (2011). The ER in 3D: a multifunctional dynamic membrane network. Trends Cell Biol. *21*, 709–717.

Ghila, L., and Gomez, M. (2008). The evolutionarily conserved gene LNP-1 is required for synaptic vesicle trafficking and synaptic transmission. Eur. J. Neurosci. *27*, 621–630.

Gorres, K.L., and Raines, R.T. (2010). Prolyl 4-Hydroxylase. Crit. Rev. Biochem. Mol. Biol. *45*, 106–124.

Goyal, U., and Blackstone, C. (2013). Untangling the web: mechanisms underlying ER network formation. Biochim. Biophys. Acta *1833*, 2492–2498.

Grigoryan, A.V., Wang, H., and Cardozo, T.J. (2012). Can the energy gap in the protein-ligand binding energy landscape be used as a descriptor in virtual ligand screening? PLoS ONE *7*, e46532.

Hara, K., Maruki, Y., Long, X., Yoshino, K., Oshiro, N., Hidayat, S., Tokunaga, C., Avruch, J., and Yonezawa, K. (2002). Raptor, a binding partner of target of rapamycin (TOR), mediates TOR action. Cell *110*, 177–189.

Jewell, J.L., Kim, Y.C., Russell, R.C., Yu, F.-X., Park, H.W., Plouffe, S.W., Tagliabracci, V.S., and Guan, K.-L. (2015). Metabolism. Differential regulation of mTORC1 by leucine and glutamine. Science *347*, 194–198.

Jin, L., Pahuja, K.B., Wickliffe, K.E., Gorur, A., Baumgärtel, C., Schekman, R., and Rape, M. (2012). Ubiquitin-dependent regulation of COPII coat size and function. Nature *482*, 495–500.

Kaneko, T., Li, L., and Li, S.S. (2008). The SH3 domain–a family of versatile peptide- and protein-recognition module. Front. Biosci. *13*, 4938–4952.

Keuss, M.J., Thomas, Y., Mcarthur, R., Wood, N.T., Knebel, A., and Kurz, T. (2016). Characterization of the mammalian family of DCN-type NEDD8 E3 ligases. J. Cell Sci. *129*, 1441–1454.

Kim, D.-H., Sarbassov, D.D., Ali, S.M., King, J.E., Latek, R.R., Erdjument-Bromage, H., Tempst, P., and Sabatini, D.M. (2002). mTOR interacts with raptor to form a nutrient-sensitive complex that signals to the cell growth machinery. Cell *110*, 163–175.

Kim, E., Goraksha-Hicks, P., Li, L., Neufeld, T.P., and Guan, K.L. (2008). Regulation of TORC1 by Rag GTPases in nutrient response. Nat. Cell Biol. *10*, 935–945.

Kurz, T., Ozlü, N., Rudolf, F., O'Rourke, S.M., Luke, B., Hofmann, K., Hyman, A.A., Bowerman, B., and Peter, M. (2005). The conserved protein DCN-1/Dcn1p is required for cullin neddylation in C. elegans and S. cerevisiae. Nature *435*, 1257–1261.

Kurz, T., Chou, Y.C., Willems, A.R., Meyer-Schaller, N., Hecht, M.L., Tyers, M., Peter, M., and Sicheri, F. (2008). Dcn1 functions as a scaffold-type E3 ligase for cullin neddylation. Mol. Cell *29*, 23–35.

Lawrence, R.E., Cho, K.F., Rappold, R., Thrun, A., Tofaute, M., Kim, D.J., Moldavski, O., Hurley, J.H., and Zoncu, R. (2018). A nutrient-induced affinity switch controls mTORC1 activation by its Rag GTPase-Ragulator lysosomal scaffold. Nat. Cell Biol. *20*, 1052–1063.

Lee, S.B., Frattini, V., Bansal, M., Castano, A.M., Sherman, D., Hutchinson, K., Bruce, J.N., Califano, A., Liu, G., Cardozo, T., et al. (2016). An ID2-dependent mechanism for VHL inactivation in cancer. Nature *529*, 172–177.

Low, T.Y., Peng, M., Magliozzi, R., Mohammed, S., Guardavaccaro, D., and Heck, A.J. (2014). A systems-wide screen identifies substrates of the SCFβTrCP ubiquitin ligase. Sci. Signal. *7*, rs8.

Luarte, A., Cornejo, V.H., Bertin, F., Gallardo, J., and Couve, A. (2018). The axonal endoplasmic reticulum: One organelle-many functions in development, maintenance, and plasticity. Dev. Neurobiol. *78*, 181–208.

Lydeard, J.R., Schulman, B.A., and Harper, J.W. (2013). Building and remodelling Cullin-RING E3 ubiquitin ligases. EMBO Rep. *14*, 1050–1061.

Manifava, M., Smith, M., Rotondo, S., Walker, S., Niewczas, I., Zoncu, R., Clark, J., and Ktistakis, N.T. (2016). Dynamics of mTORC1 activation in response to amino acids. eLife *5*, 1–21.

Marsan, E., and Baulac, S. (2018). Review: Mechanistic target of rapamycin (mTOR) pathway, focal cortical dysplasia and epilepsy. Neuropathol. Appl. Neurobiol. *44*, 6–17.

Meyer-Schaller, N., Chou, Y.C., Sumara, I., Martin, D.D., Kurz, T., Katheder, N., Hofmann, K., Berthiaume, L.G., Sicheri, F., and Peter, M. (2009). The human Dcn1-like protein DCNL3 promotes Cul3 neddylation at membranes. Proc. Natl. Acad. Sci. USA *106*, 12365–12370.

Monda, J.K., Scott, D.C., Miller, D.J., Lydeard, J., King, D., Harper, J.W., Bennett, E.J., and Schulman, B.A. (2013). Structural conservation of distinctive N-terminal acetylation-dependent interactions across a family of mammalian NEDD8 ligation enzymes. Structure *21*, 42–53.

Moriya, K., Nagatoshi, K., Noriyasu, Y., Okamura, T., Takamitsu, E., Suzuki, T., and Utsumi, T. (2013). Protein N-myristoylation plays a critical role in the endoplasmic reticulum morphological change induced by overexpression of protein Lunapark, an integral membrane protein of the endoplasmic reticulum. PLoS ONE *8*, e78235.

Neves, M.A., Totrov, M., and Abagyan, R. (2012). Docking and scoring with ICM: the benchmarking results and strategies for improvement. J. Comput. Aided Mol. Des. *26*, 675–686.

Petroski, M.D., and Deshaies, R.J. (2005). Function and regulation of cullin-RING ubiquitin ligases. Nat. Rev. Mol. Cell Biol. *6*, 9–20.

Phillips, M.J., and Voeltz, G.K. (2016). Structure and function of ER membrane contact sites with other organelles. Nat. Rev. Mol. Cell Biol. *17*, 69–82.

Pintard, L., Willems, A., and Peter, M. (2004). Cullin-based ubiquitin ligases: Cul3-BTB complexes join the family. EMBO J. *23*, 1681–1687.

Qi, H.H., Ongusaha, P.P., Myllyharju, J., Cheng, D., Pakkanen, O., Shi, Y., Lee, S.W., Peng, J., and Shi, Y. (2008). Prolyl 4-hydroxylation regulates Argonaute 2 stability. Nature *455*, 421–424.

Rondou, P., Haegeman, G., Vanhoenacker, P., and Van Craenenbroeck, K. (2008). BTB Protein KLHL12 targets the dopamine D4 receptor for ubiquitination by a Cul3-based E3 ligase. J. Biol. Chem. *283*, 11083–11096.

Rowland, A.A., Chitwood, P.J., Phillips, M.J., and Voeltz, G.K. (2014). ER contact sites define the position and timing of endosome fission. Cell *159*, 1027–1041.

Sancak, Y., Peterson, T.R., Shaul, Y.D., Lindquist, R.A., Thoreen, C.C., Bar-Peled, L., and Sabatini, D.M. (2008). The Rag GTPases bind raptor and mediate amino acid signaling to mTORC1. Science *320*, 1496–1501.

Sancak, Y., Bar-Peled, L., Zoncu, R., Markhard, A.L., Nada, S., and Sabatini, D.M. (2010). Ragulator-Rag complex targets mTORC1 to the lysosomal surface and is necessary for its activation by amino acids. Cell *141*, 290–303.

Sarbassov, D.D., Ali, S.M., Kim, D.H., Guertin, D.A., Latek, R.R., Erdjument-Bromage, H., Tempst, P., and Sabatini, D.M. (2004). Rictor, a novel binding partner of mTOR, defines a rapamycin-insensitive and raptor-independent pathway that regulates the cytoskeleton. Curr. Biol. *14*, 1296–1302.

Saxton, R.A., and Sabatini, D.M. (2017). mTOR Signaling in Growth, Metabolism, and Disease. Cell *168*, 960–976.

Scheldeman, C., Mills, J.D., Siekierska, A., Serra, I., Copmans, D., Iyer, A.M., Whalley, B.J., Maes, J., Jansen, A.C., Lagae, L., et al. (2017). mTOR-related neuropathology in mutant tsc2 zebrafish: Phenotypic, transcriptomic and pharmacological analysis. Neurobiol. Dis. *108*, 225–237.

Scott, D.C., Monda, J.K., Grace, C.R., Duda, D.M., Kriwacki, R.W., Kurz, T., and Schulman, B.A. (2010). A dual E3 mechanism for Rub1 ligation to Cdc53. Mol. Cell *39*, 784–796.

Scott, D.C., Monda, J.K., Bennett, E.J., Harper, J.W., and Schulman, B.A. (2011). N-terminal acetylation acts as an avidity enhancer within an interconnected multiprotein complex. Science *334*, 674–678.

Scott, D.C., Sviderskiy, V.O., Monda, J.K., Lydeard, J.R., Cho, S.E., Harper, J.W., and Schulman, B.A. (2014). Structure of a RING E3 trapped in action reveals ligation mechanism for the ubiquitin-like protein NEDD8. Cell *157*, 1671–1684.

Sekiguchi, T., Hirose, E., Nakashima, N., Ii, M., and Nishimoto, T. (2001). Novel G proteins, Rag C and Rag D, interact with GTP-binding proteins, Rag A and Rag B. J. Biol. Chem. *276*, 7246–7257.

Shemesh, T., Klemm, R.W., Romano, F.B., Wang, S., Vaughan, J., Zhuang, X., Tukachinsky, H., Kozlov, M.M., and Rapoport, T.A. (2014). A model for the generation and interconversion of ER morphologies. Proc. Natl. Acad. Sci. USA *111*, E5243–E5251.

Switon, K., Kotulska, K., Janusz-Kaminska, A., Zmorzynska, J., and Jaworski, J. (2017). Molecular neurobiology of mTOR. Neuroscience *341*, 112–153.

The UniProt Consortium (2017). UniProt: the universal protein knowledgebase. Nucleic Acids Res. *45* (*D1*), D158–D169.

Turrini, L., Fornetto, C., Marchetto, G., Müllenbroich, M.C., Tiso, N., Vettori, A., Resta, F., Masi, A., Mannaioni, G., Pavone, F.S., and Vanzi, F. (2017). Optical mapping of neuronal activity during seizures in zebrafish. Sci. Rep. *7*, 3025.

Villar, V.H., Merhi, F., Djavaheri-Mergny, M., and Durán, R.V. (2015). Glutaminolysis and autophagy in cancer. Autophagy *11*, 1198–1208.

Wang, S., Tukachinsky, H., Romano, F.B., and Rapoport, T.A. (2016). Cooperation of the ER-shaping proteins atlastin, lunapark, and reticulons to generate a tubular membrane network. eLife *5*, e18605.

Wilson, A.A., Kwok, L.W., Hovav, A.H., Ohle, S.J., Little, F.F., Fine, A., and Kotton, D.N. (2008). Sustained expression of alpha1-antitrypsin after transplantation of manipulated hematopoietic stem cells. Am. J. Respir. Cell Mol. Biol. *39*, 133–141.

Zhang, C., Liu, J., Huang, G., Zhao, Y., Yue, X., Wu, H., Li, J., Zhu, J., Shen, Z., Haffty, B.G., et al. (2016). Cullin3-KLHL25 ubiquitin ligase targets ACLY for degradation to inhibit lipid synthesis and tumor progression. Genes Dev. *30*, 1956–1970.

Zhao, Y., Zhang, T., Huo, H., Ye, Y., and Liu, Y. (2016). Lunapark Is a Component of a Ubiquitin Ligase Complex Localized to the Endoplasmic Reticulum Three-way Junctions. J. Biol. Chem. *291*, 18252–18262.

STAR★METHODS

KEY RESOURCES TABLE

REAGENT or RESOURCE	SOURCE	IDENTIFIER
Antibodies		
Rabbit polyclonal anti-Lunapark	Sigma-Aldrich	Cat# HPA014205; RRID:AB_2234186
Mouse monoclonal anti-KLHL12	Cell Signaling Technology	Cat# 9406; RRID:AB_2797699
Mouse monoclonal anti-FLAG	Sigma-Aldrich	Cat# F3165; RRID:AB_259529
Mouse Monoclonal anti-HA	Biolegend	Cat# 901514; RRID:AB_2565336
Rabbit polyclonal anti-GFP	Torrey Pines Biolabs	Cat# TP401; RRID:AB_10013661
Rabbit polyclonal anti-GβL(mLST8)	Cell Signaling Technology	Cat# 3274; RRID:AB_823685
Rabbit polyclonal anti-FLAG	Sigma-Aldrich	Cat# F7425; RRID:AB_439687
Rabbit polyclonal anti-βActin	Santa Cruz	Cat# sc69879; RRID:AB_1119529
Rabbit polyclonal anti-AKT	Bethyl Laboratories	Cat# A302-065A; RRID:AB_1604215
Rabbit polyclonal anti-HA	Cell Signaling Technology	Cat# 3724; RRID:AB_1549585
Rabbit polyclonal anti-phospho-p70-S6K (Thr389)	Cell Signaling Technology	Cat# 9234; RRID:AB_2269803
Rabbit polyclonal anti-p70-S6K	Bethyl Laboratories	Cat# A300-510A; RRID:AB_2182248
Rabbit polyclonal anti-Raptor	Bethyl Laboratories	Cat# A300-553A; RRID:AB_2130793
Rabbit monoclonal anti-Rictor	Cell Signaling Technology	Cat# 2114; RRID:AB_2179963
Rabbit monoclonal anti-Deptor/DEPDC6	Cell Signaling Technology	Cat# 11816; RRID:AB_2750575
Rabbit monoclonal anti-mTOR	Cell Signaling Technology	Cat# 2983; RRID:AB_2105622
Mouse monoclonal anti-mTOR	Merck-Millipore	Cat# 05-1592; RRID:AB_1977357
Mouse monoclonal anti-LAMP2/CD107b	Novus Biologicals	Cat# NBP2-22217SS; RRID:AB_2722697
Rabbit polyclonal anti-Calreticulin	Abcam	Cat# ab2907; RRID:AB_303402
Mouse IgG, HRP-linked whole Ab (from sheep)	GE Healthcare	Cat# NA931; RRID:AB_772210
Rabbit IgG, HRP-linked whole Ab (from donkey)	GE Healthcare	Cat# NA934; RRID:AB_772206
Mouse monoclonal anti-Myc	Sigma-Aldrich	Cat# M5546; RRID:AB_260581
Chemicals, Peptides, and Recombinant Proteins		
Proteasome Inhibitor MG132	Peptide Institute	Cat# 3175-V
Lipofectamine RNAiMAX	Thermo Fisher Scientific	Cat# 13778075
MLN-4924	Active Biochem	Cat# 1139
Cycloheximide	Sigma Aldrich	Cat# C104450
Experimental Models: Cell Lines		
Human U2OS	ATCC	Cat# HTB-96; RRID:CVCL_0042
Human HEK293T	ATCC	Cat# CRL-11268; RRID:CVCL_1926
Human HeLa	ATCC	Cat# CCL-2; RRID:CVCL_0030
Oligonucleotides		
Human KLHL12 siRNA targeting sequence	Dharmacon	Cat# 2958852
Recombinant DNA		
mCherry-Sec61β	Addgene plasmids	Cat# 49155; RRID:Addgene_49155
Rtn4a-GFP	Addgene plasmids	Cat# 61807; RRID:Addgene_61807
LAMP1-GFP	Addgene plasmids	Cat# 34831; RRID:Addgene_34831
LAMP1-mCherry	Addgene plasmids	Cat# 45147; RRID:Addgene_45147
pAc-GFPC1-Sec61β	Addgene plasmids	Cat# 15108; RRID:Addgene_15108
pRK5-HA-mCherry-RAPTOR	Addgene plasmids	Cat# 73386; RRID:Addgene_73386
pcDNA3-FLAG-FLAG-HA-HA-Lunapark	This paper	N/A
pHAGE2-EF1α-IRES-Lunapark	This paper	N/A
pcDNA3-2xFLAG-CUL3-N225	This paper	N/A
pcDNA3-2xFLAG-CUL3-N225-MB	This paper	N/A

(*Continued on next page*)

Continued

REAGENT or RESOURCE	SOURCE	IDENTIFIER
pcDNA3-FLAG-CUL3-N199-MB	This paper	N/A
pcDNA3-FLAG-CUL3-N199	This paper	N/A
pWC7-His-MYC-ubiquitin	This paper	N/A
pcDNA3-Lunapark-HA	This paper	N/A
pcDNA-FLAG-KLHL12	This paper	N/A
Critical Commercial Assays		
QuickChange Site-Directed Mutagenesis Kit	Stratagene	Cat# 200518
Software and Algorithms		
ImageJ	https://imagej.nih.gov/ij/	https://imagej.nih.gov/ij/ ; RRID:SCR_003070

RESOURCE AVAILABILITY

Lead Contact

Further information and requests for resources and reagents should be directed to and will be fulfilled by the Lead Contact, Daniele Guardavaccaro. (daniele.guardavaccaro@univr.it).

Materials Availability

All unique/stable reagents generated in this study are available from the Lead Contact with a completed Materials Transfer Agreement. Commercially available reagents are indicated in the Key Resources Table.

Data and Code Availability

This article includes all datasets/code generated or analyzed during this study (Tables S1 and S2).

EXPERIMENTAL MODEL AND SUBJECT DETAILS

Human cells, transfection and drug treatment

HEK293T, HeLa, U2OS and hTERT-RPE cells were maintained in Dulbecco's modified Eagle's medium (DMEM; Thermo Fisher Scientific) containing 10% fetal calf serum, 100 U/ml penicillin, and 100 μg/ml streptomycin. Cells were transfected by the polyethylenimine (PEI) method. siRNA oligonucleotide against human KLHL12 was purchased from Dharmacon (Clone ID: 2958852) and transfected into cells using Lipofectamine RNAiMAX (Thermo Fisher Scientific) according to manufacturer's protocol. The following drugs were used: MG132 (Peptide Institute, 10 μM), MLN4924 (Active Biochemicals, 0.5 μM), and cycloheximide (Sigma-Aldrich, 100 μM).

Zebrafish embryo injections and analysis

Wild-type and transgenic [Tg(Elavl3:GCaMP6)] zebrafish lines were maintained under standard husbandry conditions and mated according to standard procedures at the Interdepartmental Centre for Experimental Research (CIRSAL) of the University of Verona. mRNAs for injection were transcribed using the mMESSAGE mMACHINE SP6 Transcription Kit (ThermoFisher Scientific-Ambion) using linearized pCS2+ constructs as template. One-cell stage zebrafish embryos were injected with 2.5 pg of mRNA [wild-type Lunapark or Lunapark(P204A/P207A)] as previously described (Astone et al., 2018). Injected fish were screened to detect the presence of phenotypic alterations including evident morphological distortion, cardiac edema, abnormalities of head, eye, tail and fin by visual assessment.

For brain analysis, the Tg(Elavl3:GCaMP6) transgenic reporter line, which displays robust transgene expression in the brain at 2 dpf, was employed (Turrini et al., 2017). Two dpf injected embryos were positioned dorsally in 3% methylcellulose on a microscope slide. Images were taken using a LEICA MZ16F fluorescence microscope and the Leica Application Suite V4.12 software. The brain size was measured using the Fiji-ImageJ software and normalized against the body length. GraphPad Prism was used to conduct statistical analysis (Student's t test). For locomotion analysis, 4 dpf injected larvae were placed individually in wells of a 24-well flat-bottomed culture dish. Locomotion was tracked for 30 minutes in basal condition followed by 45 minutes of recording after administration of 1.25 mM pentylenetetrazole (PTZ) at 28.5°C using a DanioVision system (Noldus) consisting of an isolated chamber with an infrared camera. Both the distance traveled and the velocity of swimming were analyzed using the EthoVision XT-15 locomotion tracking software. GraphPad Prism was used for statistical analysis (Student's t test). Differences were considered significant if $p < 0.05$. All experiments were carried in accordance to the Italian law on animal experimentation (D.L. 4 March 2014, n.26), under authorization n°186474 (27/05/2019).

METHOD DETAILS

Plasmids, cloning and lentivirus production

The Cullin-3 deletion mutants CUL3-N199 and CUL3-N225 carrying one or two C-terminal FLAG tags, respectively, were generated by PCR and subcloned into the pcDNA3 vector. The membrane-targeted Cullin-3 mutants (CUL3-N199-MB and CUL3-N225-MB) were constructed by fusing the first 11 amino acids of DCNL3 (Meyer-Schaller et al., 2009) to the N-terminal of the CUL3 deletion mutants by PCR. Human Lunapark and KLHL12 cDNAs were obtained from GE Healthcare. Lunapark carrying C-terminal 2xFLAG-2xHA or a single HA and KLHL12 carrying an N-terminal FLAG were subcloned into pcDNA3. Deletion mutants of Lunapark (ΔMs, ΔZFM, ΔC) and KLHL12 (ΔKelch1-3, ΔKelch4-6) were generated by PCR and subcloned into pcDNA3. The HA-tagged Lunapark(P204A/P207A) was generated by site-directed mutagenesis (Stratagene). Lunapark WT, ΔM2 and P204A/P207A were also subcloned into pEGFP-N1. mCherry-Sec61β (Addgene plasmids # 49155) and Rtn4a-GFP (Addgene plasmids # 61807) were gifts from Gia Voeltz, LAMP1-GFP (Addgene plasmids # 34831) was a gift from Esteban Dell'Angelica, LAMP1-mCherry (Addgene plasmids # 45147) was a gift from Amy Palmer, pAc-GFPC1-Sec61β (Addgene plasmids # 15108) was a gift from Tom Rapoport, pRK5-HA-mCherry-RAPTOR (Addgene plasmids # 73386) was a gift from Jie Chen and Taekjip Ha. For lentiviral transduction, wild-type Lunapark and mutants were subcloned into pHAGE2-EF1α-IRES-puromycin vectors (Wilson et al., 2008). For lentiviral transduction, HEK293T cells were transfected by the polyethylenimine (PEI) method with the pHAGE2 vector together with packaging vectors encoding Gag-Pol, Rev, Tat, and the G protein of the vesicular stomatitis virus (VSV). Supernatants were collected every 48 hours on two consecutive days starting 24 hours after transfection, filtered and transferred to cells in the presence of polybrene (4 μg/ml).

Identification of CUL3 and Lunapark interactors

HEK293T cells were transfected with pcDNA3-FLAG-CUL3-N199, pcDNA3-2xFLAG-CUL3-N225, pcDNA3-FLAG-CUL3-N199-MB, pcDNA3-2xFLAG-CUL3-N225-MB or pcDNA3-Lunapark-2xFLAG-2xHA. Cells were harvested and subsequently lysed in lysis buffer [50 mM Tris-HCl (pH 7.5), 150 mM NaCl, 1 mM EDTA, and 0.5% NP-40 plus protease and phosphatase inhibitors]. CUL3 and Lunapark were immunopurified with anti-FLAG agarose resin (Sigma-Aldrich). The beads were washed and proteins were eluted using RapiGest SF (Waters). Eluents were subsequently treated with reduction buffer (1 μg/μl dithiothreitol) for 30 minutes and alkylation buffer (5 μg/μl iodoacetamide) for 20 minutes, followed by Lys-C for 4 hours. Trypsin was then added at the 1:50 ratio and mixture was incubated overnight at 37°C. Trypsin was quenched by adding trifluoroacetic acid (TFA). The mixture was then subjected to C18 SEP-PAK desalting.

For MS analysis, peptides were first separated with a C18 column (Zorbax) and introduced by nanoelectrospray into the LTQ Orbitrap Elite (Thermo Fisher) and MS/MS in data-dependent decision tree mode (collision-induced dissociation/electron transfer dissociation) as described previously (Low et al., 2014). Raw files were converted to MGF files using Proteome Discoverer version 1.4 (Thermo Fisher). The non-fragment filter was used to simplify ETD spectra and the Top N filter (6 highest peaks admitted per 100 Da) for the CID spectra. All MGF files were submitted to Mascot search engine (version 3.0) via Proteome Discoverer version 1.4. The spectra were searched against the UniProt Human database (version 2013-07, 20,277 entries). Trypsin/P was chosen as the protease with 2 missed cleavages, cysteine carbamidomethylation was set as fixed modification; and oxidation of methionine and acetylation of the N terminus of the protein were set as variable modifications. Peptide tolerance was set to 15 ppm and MS/MS tolerance set to 0.5 dalton. All peptide-spectrum matches (PSMs) were filtered at a Mascot score cutoff at 30. Only PSMs with a minimum length of 7 amino acids were kept. To normalize spectral count data, we exported the full list with Normalized Spectral Abundance Factors (NSAF). NSAF is calculated as the number of spectral counts (SpC) identifying a protein, divided by the protein's length (L), in turn divided by the sum of SpC/L for all proteins in the experiment.

CRISPR genome editing

To generate *LNPK*$^{-/-}$ cell lines, two optimal gRNA target sequences targeting both exon 1 and exon 13 (genomic deletion) were designed using the Benchling CRISPR Genome Engineering tool and cloned into pSpCas9(BB)-2A-GFP (PX458). U2OS cells were seeded into 10-cm dishes at approximately 70% confluency and transfected with 2.5 μg of both gRNA-containing PX458 plasmids using the polyethylenimine (PEI) method. Two days after transfection, GFP-positive cells were sorted using the BD FACSJazz™ cell sorter, and 20 cells/well were plated in a 96-well plate. One to two weeks later, single cell clones were picked, trypsinized in 0.25% Trypsin-EDTA for 5 minutes, and plated into individual wells of a 96-well plate for genotyping. Genomic DNA was collected using DNA lysis buffer (100 mM Tris-HCl pH 8.0, 200 mM NaCl, 5 mM EDTA pH 8.0, 0.2% SDS) supplemented with 10 μg/μl proteinase K. Genotyping PCRs were performed with GoTaq G2 Flexi DNA Polymerase (Promega), using primers surrounding the genomic target sites. Positive clones were sequenced to determine the presence of deletion event (*LNPK* knockout). To further validate the mutational status of candidate clones, single clones were screened for Lunapark expression by immunoblotting.

Biochemical methods

For preparation of cell extracts, cells were washed and collected in ice-cold PBS and lysed in Triton-X lysis buffer (50 mM Tris pH 7.5, 250 mM NaCl, 0.1% Triton X-100, 1 mM EDTA, 50 mM NaF and protease and phosphatase inhibitors) for 30 minutes on ice, followed by centrifugation for 20 minutes at 4°C. Cell extracts were then submitted to either immunoblotting or immunoprecipitation followed by immunoblotting. For immunoprecipitation, cell extracts were first precleared by incubation with protein G- or protein A-Sepharose

beads (Thermo Fisher Scientific) for 45 minutes at 4°C. Precleared extracts were incubated with the indicated antibody for 3 hours at 4°C followed by protein G- or protein A-Sepharose beads for 45 minutes. Beads were washed 4 times with lysis buffer and proteins were eluted in 5x Laemmli sample buffer [50mM Tris-HCl, pH 6,8, 2% (w/v) SDS, 5% (v/v), β-mercaptoethanol, 0,1% (w/v) bromophenol blue and 1% (v/v) glycerol]. The immunoprecipitation in the presence of the crosslinking agent dithiobis (succinimidyl propionate)(DSP) (Thermo Fisher Scientific PG82081) was performed as previously described (Kim et al., 2002). For immunoblotting, proteins were separated by SDS-polyacrylamide gel electrophoresis (SDS-PAGE), transferred onto PVDF membranes (Merck-Millipore), and incubated with the indicated antibodies. For ubiquitylation assay in cultured cells, HEK293T cells were transfected with pcDNA3-Lunapark-HA (WT or mutants), pcDNA-FLAG-KLHL12 (WT or ΔKelch4-6), or pWC7-His-MYC-ubiquitin (WT or K-less), as indicated. Forty-eight hours later, cells were treated with MG132 for 4 hours before harvesting. Cells were lysed in RIPA buffer (25 mM Tris pH 7.5, 150 mM NaCl, 1% NP40, 1% sodium deoxycholate, 0.1% SDS and protease and phosphatase inhibitors) and subjected to immunoprecipitation using c-Myc antibody. Ubiquitylated Lunapark was detected by immunoblotting using an anti-Lunapark antibody.

Antibodies

The following antibodies were used in this study: anti-Lunapark, rabbit polyclonal (Sigma-Aldrich, HPA014205), anti-KLHL12, mouse monoclonal (Cell Signaling Technology, 9406), anti-FLAG, rabbit polyclonal (Sigma-Aldrich, F7425), anti-FLAG, mouse monoclonal (Sigma-Aldrich, F7425), anti-HA, mouse monoclonal (Biolegend, 901514), anti-HA, rabbit monoclonal (Cell Signaling Technology, 3724), anti-β-actin, mouse monoclonal (Santa Cruz, sc-69879), anti-Myc, mouse monoclonal (Sigma-Aldrich, M5546), anti-GFP, rabbit polyclonal (Torrey Pines Biolabs, TP401), anti-GβL(mLST8), rabbit monoclonal (Cell Signaling Technology, 3274), anti-AKT, rabbit polyclonal (Bethyl Laboratories, A302-065A), anti-phospho-p70-S6K (Thr389), rabbit monoclonal (Cell Signaling Technology, 9234), anti-p70-S6K, rabbit polyclonal (Bethyl Laboratories, A300-510A), anti-Raptor, rabbit polyclonal (Bethyl Laboratories, A300-553A), anti-Rictor, rabbit monoclonal (Cell Signaling Technology, 2114), anti-Deptor/DEPDC6, rabbit monoclonal (Cell Signaling Technology, 11816). Anti-mouse IgG (NA931) and anti-rabbit IgG (NA934) horseradish peroxidase (HRP) conjugated secondary antibodies were from GE Healthcare. The following primary antibodies were used for immunofluorescence and proximity ligation assays: anti-HA, mouse monoclonal (Biolegend, 901514), anti-mTOR, rabbit monoclonal (Cell Signaling Technology, 2983), anti-mTOR, mouse monoclonal (Merck-Millipore, 05-1592), anti-LAMP2/CD107b, mouse monoclonal (Novus Biologicals, NBP2-22217SS) and anti-Calreticulin, rabbit polyclonal (Abcam, ab2907). Alexa Fluor 488-, Alexa Fluor 568- or Alexa Fluor 594-conjugated secondary antibodies were from Thermo Fisher Scientific.

Immunofluorescence

Cells were seeded on polylysine-L (Sigma-Aldrich) treated glass coverslips and, when specified, transfected with the indicated plasmids. One day after transfection, cells were fixed with 4% paraformaldehyde (PFA), permeabilized with 0.1% Triton X-100 in PBS and incubated with primary antibodies for 1.5 hours at room temperature. Cells were washed three times using 0.5% Tween-20 in PBS (PBS-T) and incubated with Alexa Fluor 488-, Alexa Fluor 568- or Alexa Fluor 594-conjugated secondary antibodies (Thermo Fisher Scientific) for 1 hour at room temperature. Cells were washed three times with PBS-T and slides were mounted using the Vectashield antifade mounting medium (Vector Laboratories). Fluorescence images were acquired on a Leica DM6000 fluorescence microscope and analyzed using the ImageJ (NIH) software. The colocalization plugin in ImageJ was used to visualize co-localization between two channels (thresholds were set equal for all images analyzed).

In situ proximity ligation assay (PLA)

Cells were seeded on glass coverslips treated with polylysine-L (Sigma-Aldrich). After 24 hours, cells were fixed with 4% paraformaldehyde (PFA) and permeabilized with 0,1% Triton X-100 in PBS. The PLA assay was performed according to the manufacturer's protocol (Duolink *In situ* Red, Sigma-Aldrich DUO92101-1KT). Briefly, following permeabilization, the coverslips were subjected to blocking, incubation with primary antibodies for 1.5 hours at room temperature, hybridization with PLA probes, ligation, amplification and counterstaining with mouse monoclonal anti-α-tubulin antibody-FITC (Sigma-Aldrich F2168) before mounting. Fluorescent images were acquired on a Leica DM6000 fluorescence microscope and analyzed using the ImageJ software (NIH). The number of PLA punctae, indicative of a direct interaction between Lunapark and mTOR, were counted for all three conditions ($n < 20$ cells). P values were determined by unpaired, two-tailed Student's t test using Graphpad Prism 7. P values < 0.05 are indicated with one asterisk, < 0.01 with two asterisks, < 0.001 with three asterisks and < 0.0001 with four asterisks, respectively.

Live cell imaging by spinning disc confocal microscopy

U2OS cells were grown in glass bottom dishes and transfected with mCherry-Sec61β, Lunapark-GFP (WT or mutants), mCherry-Raptor, mCherry-LAMP1 or GFP-LAMP1. One day after transfection, cells were imaged using a Nikon-SD spinning disk confocal microscope. The movies were generated using the ImageJ software (NIH). The multichannel plot profile function in ImageJ was used to obtain line-scan graphs representing the relative fluorescence intensity of the mCherry and GFP channels along the length (linear distance in pixels) of a line drawn in ImageJ. For triple-labeled live cell imaging, U2OS cells were transfected with Lunapark-GFP, BFP-KDEL (ER marker) and mCherry-LAMP1 (lysosome marker). One day after transfection, cells were imaged using a Leica TCS SP5 AOBS (Acousto-Optical Beam Splitter) confocal microscope and analyzed using the ImageJ (NIH) software.

In vitro binding assay

In vitro translated ^{35}S-labeled KLHL12 or KLHL18 were incubated with protein G-Sepharose beads precoupled with the following Lunapark synthetic peptides: H-DSSAPGGPPERTVT-OH, or H-DSSAAGGAPERTVT-OH for 2 hours at 4°C. Beads were washed four times with lysis buffer (50 mM Tris-HCl, pH 7.4, 1 mM EDTA, 250 mM NaCl, 0.1% Triton X-100, 50 mM NaF, 1 mM DTT, 0.1 mM Na_3VO_4). Proteins were then eluted with Laemmli buffer for 3 minutes at 95°C and subjected to SDS-PAGE followed by autoradiography.

Computational molecular docking of Lunapark peptide to KLHL12

A highly accurate, flexible peptide docking method (ICM-Pro, Molsoft LLC, La Jolla CA) was used as previously described (Bordner and Abagyan, 2006; Lee et al., 2016) to dock Lunapark peptides to KLHL12. Full atom models of Lunapark peptides were docked to grid potential maps generated from the atomic coordinates of the Kelch repeats of KLHL12 reported in the crystallographic structure of KLHL12 (Canning et al., 2013). The all-atom model of the peptide was docked into the grid potentials using stochastic global optimization in internal coordinates with pseudo-Brownian and collective 'probability-biased' random moves as implemented in the ICM-Pro program. For the grids, five types of potentials for the peptide-receptor interaction energy - hydrogen van der Waals, non-hydrogen van der Waals, hydrogen bonding, hydrophobicity and electrostatics - were precomputed on a rectilinear grid with 0.5 Å spacing that fills a 34 Å × 34 Å × 25 Å box containing KLHL12, to which the peptide was docked by searching its full conformational space within the space of the grid potentials. The preferred docking conformation was identified by the lowest energy conformation in the search.

QUANTIFICATION AND STATISTICAL ANALYSIS

GraphPad Prism was used for statistical analysis (Student's t test). Sample sizes and *p* values are indicated in STAR Methods, figures or figure legends. All images are representative of at least three biological replicates, except where specified in the figure legends.